Progress in the analysis of experimental chaos through periodic orbits

R. Badii

Paul Scherrer Institute, CH-5232 Villigen, Switzerland

E. Brun

Physics Institute, University of Zürich, CH-8057 Zürich, Switzerland

M. Finardi

Paul Scherrer Institute, CH-5232 Villigen, Switzerland

L. Flepp, R. Holzner, J. Parisi, C. Reyl, and J. Simonet

Physics Institute, University of Zürich, CH-8057 Zürich, Switzerland

The understanding of chaotic systems can be considerably improved with the knowledge of their periodic-orbit structure. The identification of the low-order unstable periodic orbits embedded in a strange attractor induces a hierarchical organization of the dynamics which is invariant under smooth coordinate changes. The applicability of this technique is by no means limited to analytical or numerical calculations, but has been recently extended to experimental time series. As a specific example, the authors review some of the major results obtained on a nuclear-magnetic-resonance laser which have led to an extension of the conventional (Bloch-Kirchhoff) equations of motion, to the construction of approximate generating partitions, and to an efficient control of the chaotic system around various unstable periodic orbits. The determination of the symbolic dynamics, with the precision achieved by recording all unstable cycles up to order 9, improves the topological and metric characterization of a heteroclinic crisis. The periodic-orbit approach permits detailed study of chaotic motion, thereby leading to an improved classification scheme which subsumes the older ones, based on estimates of scalar quantities such as fractal dimensions and metric entropies.

CONTENTS

I. Introduction 1389
II. Periodic Orbits and Hierarchical Encoding 1391
III. The NMR Laser and its Mathematical Model 1395
A. Spin dynamical aspects of ruby 1396
B. Conventional Bloch equations for the NMR laser 1397
C. Extended Bloch-type laser equations 1398
D. Chaotic laser behavior 1400
IV. Model-Experiment Comparison 1400
A. Basic test of the extended Bloch-type laser model 1400
B. Conventional analysis of chaotic motion 1402
C. Periodic orbits 1405
D. Crisis 1407
V. Control of the Chaotic Flow 1409
VI. Summary and Outlook 1412
Acknowledgments 1412
References 1412

I. INTRODUCTION

Although the discovery of deterministic chaos can be dated back to the work of the mathematician H. Poincaré (1892), the relevance of this phenomenon has been recognized only recently, mainly as a result of investigations on the nature of turbulence (Lorenz, 1963; Ruelle and Takens, 1971). For a long time, in fact, the study of systems that are now called chaotic remained confined to mathematics or to specialized branches of physics (Kolmogorov, 1954; Arnold, 1964; Šarkovskii, 1964; Smale, 1967; Arnold and Avez, 1968; Shilnikov, 1970; Metropolis *et al.*, 1973; Moser, 1973; Chirikov, 1979). It was, however, only with Feigenbaum's explanation of the period-doubling transition to chaos in terms of a universal mechanism (Feigenbaum, 1978, 1979, 1980) that the study of chaos became a popular subject of theoretical physics. Feigenbaum's theory received widespread acknowledgment after experimental confirmation (Libchaber and Maurer, 1979), although its formal elegance had already been appreciated. Since then, the study of chaos has undergone a dramatic expansion which has deeply influenced fields as diverse as hydrodynamics, optics, celestial mechanics, engineering, chemistry, economy, and biology (Haken, 1981; Swinney and Gollub, 1981; Cvitanović, 1984; Bergé *et al.*, 1986; Guckenheimer and Holmes, 1986; Mayer-Kress, 1986; Schuster, 1988; Lichtenberg and Lieberman, 1992; Abarbanel *et al.*, 1993). These disciplines are now commonly regrouped under the term "nonlinear science" (Drazin and King, 1992; Zaslavsky *et al.*, 1991; Beck and Schlögl, 1993; McCauley, 1993; Nakamura, 1993). The unifying thread among them is the nonlinearity of the forces. Even more important, a large portion of the interesting natural phenomena arises from nonlinearity without necessarily being chaotic.

 0034-6861/94/66(4)/1389(27)/$07.70

The paradigm of chaos is the well-known sensitivity to initial conditions: two orbits in phase space starting at a distance ε, much smaller than the typical size of the region visited during the motion, diverge exponentially in time, so that their separation after a time t will be of the order of $\varepsilon e^{\lambda t}$ with λ a positive, real number. This makes long-time predictions virtually impossible. A suitable average of the exponential growth rate λ, the Lyapunov exponent, represents one of the most common indicators of chaotic behavior (Eckmann and Ruelle, 1985). This instability does not prevent the system trajectories from remaining confined in a bounded domain of phase space when the nonlinearity provides a sufficiently strong folding mechanism. Chaotic motion exhibits contraction, as well as expansion. Accordingly, each of the d eigendirections of the linearized flow at some point $\mathbf{x}$ in phase space carries a local Lyapunov exponent $\lambda_i(\mathbf{x})$ $(i=1,\ldots,d)$. A global characterization of the stability properties of the system under infinitesimal perturbations is obtained by evaluating the average Lyapunov exponents over the chaotic trajectory (Oseledec, 1968; Pesin, 1976). The signature for chaos is the positivity of at least one of them. The sum γ of the average Lyapunov exponents represents the volume variation rate in time, which can be expressed as $V(t)\approx V(0)\exp(\gamma t)$. It is customary to distinguish between conservative (volume-preserving) systems, having $\gamma=0$, and dissipative systems, having $\gamma<0$. Research in these two fields has evolved in parallel. We concentrate on the dissipative case. For a review of conservative chaotic behavior, see MacKay and Meiss (1987) and Lichtenberg and Lieberman (1992).

The combined effect of stretching and folding is responsible, in dissipative systems, for the creation of strange attractors: zero-volume sets of points having locally the topology of products between continuous curves and Cantor sets. These objects are invariant under the dynamics and exhibit a dimension D which, besides being smaller than that of the phase space, can take noninteger values (Young, 1982; Eckmann and Ruelle, 1985; Mayer-Kress, 1986). The evaluation of such a "fractal" dimension (Mandelbrot, 1982) has been one of the most popular characterizations of strange attractors in the last decade (Grassberger and Procaccia, 1983, 1984; Badii and Politi, 1984, 1985; Mayer-Kress, 1986).

Finally, the average information about the initial conditions obtained by observing the motion in a unit of time is appropriately measured by the Kolmogorov-Sinai or metric entropy K_1 (Billingsley, 1965; Cornfeld *et al.*, 1982; Walters, 1985). In fact, all initial conditions belonging to a small domain of size $\varepsilon>0$, below the experimental resolution, will evolve into distinguishable (i.e., ε separated) states after a finite time t, because of the exponential divergence of nearby orbits (Eckmann and Ruelle, 1985). New information is revealed by the stretching mechanism. Relations can be found between dimension, entropy, and Lyapunov exponents (Grassberger *et al.*, 1988). Since these average indicators only provide a global characterization of the dynamics, extensions of them have been introduced to account for the fluctuations of the associated local quantities on the invariant set (Renyi, 1970; Grassberger and Procaccia, 1984; Grassberger *et al.*, 1988). In fact, measurements of orbit divergency, dimension, and information yield different results in different positions in phase space if performed with a finite resolution.

It has long been recognized that, with a suitable definition of the local domains, the averaging procedures are equivalent to thermodynamic sums (Sinai, 1972; Bowen, 1975; Ruelle, 1978; Halsey *et al.*, 1986; Grassberger *et al.*, 1988; Beck and Schlögl, 1993). Methods for the estimation of these quantities from (experimental or numerical) time series have been applied with quite satisfactory results (Grassberger *et al.*, 1991). The accuracy of the estimates is limited by the dimension D of the invariant set (the so-called low-dimensional chaos, with $D\leq 4$, is relatively easy to handle), by the number N of available data, and, in the case of experiments, by the presence of noise. In particular, the distinction between deterministic chaos and randomness is currently a subject of intense research (see Grassberger *et al.*, 1993, for a review). The limitations of this approach are not only of a practical nature. The analysis of data produced by nonlinear systems must be sufficiently accurate to account also for behavior that, although not chaotic, appears too complex to be understood with standard statistical tools such as probability distributions or correlation functions. Often-quoted examples are fractal aggregates (Meakin, 1990), spiral patterns in chemical reactions (Jahnke *et al.*, 1989), quasicrystals (Steinhardt and Ostlund, 1987), cellular automata (Wolfram, 1986), DNA molecules (Lewin, 1990), and spin glasses (Mézard *et al.*, 1987). In spite of the apparent dissimilarity of these fields, a common description can be achieved by introducing a symbolic encoding of the patterns (when they are not already given in a discrete form). Nonlinear dynamical systems fit into this scheme, since they exhibit behavior ranging from periodic or quasiperiodic to chaotic, including intermediate forms of aperiodicity observed at the transition to chaos. This apparently heterogeneous collection of problems is now regrouped under the heading "complex systems," and is raising growing interest. The coexistence of ordered and irregular features in these systems points out the need for novel indicators in order to achieve a classification of the broader range of phenomena that are presently facing the researcher (Grassberger, 1986; Abraham *et al.*, 1989; Stein, 1989). Most of the recent definitions of complexity (Grassberger, 1986; Badii, 1989b and 1990; Crutchfield and Young, 1989; D'Alessandro and Politi, 1989) are based on properties of stationary symbol sequences. In nonlinear dynamics, such analysis is possible if the trajectories of the system are suitably encoded with the help of a finite partition of phase space. The choice of the appropriate partition is a delicate matter which is still unresolved in its general formulation. When the symbolic encoding is possible, the trajectories can be ordered in a

hierarchical way.

Detailed information about the dynamics can be obtained, especially in low-dimensional systems, by considering the recurrent properties of the system and, in particular, by locating its unstable periodic orbits (Auerbach *et al.*, 1989; Cvitanović, 1988; Chaos, 1992). In fact, chaotic motion can be seen as an aperiodic wandering among an infinity of unstable periodic orbits, remnants of attracting cycles that bifurcated as a consequence of some parameter change in the system. The newly generated stable cycles undergo the same fate upon further variation of the external conditions, until a strange attractor is left: this is the closure of the set of the unstable periodic orbits (in the hyperbolic case; Eckmann and Ruelle, 1985). The unstable cycles can be seen as a sort of skeleton supporting the dynamics in phase space. In particular, they provide an invariant topological characterization of the dynamics. It has been proposed that knowledge of them be used to obtain a more accurate and complete description of the system. Among the many possible applications of this information are the improvement of the convergence of thermodynamic sums (Artuso *et al.*, 1990); the approximation of invariant measures (Grebogi *et al.*, 1988); the estimate of dimensions (Grebogi, Ott, and Yorke, 1987) and entropies (Lathrop and Kostelich, 1989); the analysis of transient chaos (Cvitanović, 1988; Tél, 1988; Feigenbaum *et al.*, 1989) and quasiperiodic transitions to chaos (Gunaratne *et al.*, 1988); finite-time predictions about the system evolution (Farmer and Sidorowich, 1987; Pawelzik and Schuster, 1991); noise reduction (Kostelich and Yorke, 1988); the estimate of geometrical features such as torsion and linking numbers which allow reconstruction of a three-dimensional template of the flow (Mindlin *et al.*, 1990; Tufillaro, Holzner, Flepp, Finardi, and Badii, 1991; Tufillaro, Reilly, and Abbot, 1991); and perturbation of the motion in phase space so that it approaches a desired periodic behavior (Ott *et al.*, 1990a, 1990b; Reyl *et al.*, 1993). Notwithstanding the great promises of these methods, many difficulties remain. In nonhyperbolic systems, for example, certain thermodynamic averages based on cycle expansions (Artuso *et al.*, 1990) may be less effective than direct evaluations (Grassberger *et al.*, 1990).

In this work, we illustrate several successful applications of the periodic orbit analysis when applied to experimental time series. Specifically, we focus on a system characterized by good stability properties and low noise levels which, in addition, can operate under quite different conditions, thus allowing for several types of chaotic behavior. This is the ruby NMR laser (Bösiger *et al.*, 1977), for which a mathematical model is available in the form of a low-dimensional set of differential equations (Bloch-Kirchhoff). Quantitative comparison between theory and experiment is hence possible, and it will constitute the main subject of the first part of this review. In particular, it will be shown how the identification of the periodic orbit structure helped in the finding of an improved model for the dynamics. After illustrating a method for the detection of the unstable cycles, we employ their natural hierarchical organization to obtain approximate generating partitions (Badii, 1989b, 1990, 1993; Badii *et al.*, 1991, 1992) (Sec. II). The NMR laser and its mathematical models are discussed in Sec. III. A comparison of the model with experimental results, using both standard methods and periodic orbits, is presented in Sec. IV, where symbolic dynamics is applied to the study of a heteroclinic crisis (Grebogi, Ott, Romeiras, and Yorke, 1987; Finardi *et al.*, 1992). Control of the chaotic flow (i.e., the systematic stabilization of the experimental system near an unstable periodic orbit) is illustrated in Sec. V. A summary and an overview of future research conclude our survey (Sec. VI).

II. PERIODIC ORBITS AND HIERARCHICAL ENCODING

The data recorded from an experiment typically consist of a scalar time series $\{x_k\}$ where $x_k = f(k\Delta t)$ is the value of an observable f at time $t_k = k\Delta t$ ($k = 1,2,\ldots$). A faithful reconstruction of the dynamics can be obtained by embedding the time series in a Euclidean space with sufficiently large dimension E (Takens, 1981; Sauer *et al.*, 1991). This is usually achieved by forming vectors of the type $\mathbf{x}_{k+\tau} = (x_{k+\tau}, x_{k+2\tau}, \ldots, x_{k+E\tau})$, the coordinates of which are delayed values of the observable (Packard *et al.*, 1980): the integer $\tau \geq 1$ sets the delay time $T_d = \tau\Delta t$. With an infinite amount of noise-free data, this representation is diffeomorphic to the original phase portrait if $E \geq 2D + 1$, where D is the dimension of the invariant set. Limitations in both precision and number of the data require a careful choice of the delay time T_d. Usually, a good compromise is $T_d \approx T_0/4$, where T_0 is the shortest characteristic time of the deterministic (i.e., noise-free) dynamics: for example, the length of the shortest unstable periodic orbit. In systems subjected to a periodic external force $\mathbf{A}(t)$, T_0 is just the period of $\mathbf{A}$.

Unstable periodic orbits can be located most directly by the method of close returns, i.e., by looking at orbits that form nearly closed loops (Lathrop and Kostelich, 1989; Mindlin and Gilmore, 1992). We have implemented this basic procedure with a number of improvements aimed at reducing the number of both *missed* returns and *apparent* returns (i.e., those that do not correspond to actual periodic orbits). In order to detect an orbit of period T, the trajectory in embedding space has been followed starting from some point $\mathbf{x}$ until it returned into a ball $B_\varepsilon(\mathbf{x})$ of radius ε around $\mathbf{x}$ after a time $T(\mathbf{x};\varepsilon)$ lying in the interval $[T(1-\eta), T(1+\eta)]$, where η is a free tolerance parameter. The precision ε with which the detected recurrent orbit shadows the actually periodic one has been chosen to vary with the position in phase space in order to minimize the relative error in the search (Finardi, 1993). In fact, the attractor may exhibit regions with a high density of points, where high precision is required, and others in which distinguishing different trajectories is relatively easy because of the large distance among them.

Since the data are sampled at a fixed rate $\nu=1/\Delta t$, consecutive points in the embedding space are distant from one other where the velocity is high and close together when the velocity is low. Accordingly, the ball radius $\varepsilon_i=\varepsilon(\mathbf{x}_i)$ has been chosen as

$$\varepsilon_i^2=a_1\frac{1}{\tau}\sum_{k=i-\tau/2}^{i+\tau/2}\|\mathbf{x}_k-\mathbf{x}_{k-1}\|^2 , \tag{1}$$

where $a_1\approx 0.5$ is a free parameter. In this way, the size of the ball is slightly smaller than the distance between successive data points on the trajectory: it is thus nearly proportional to $\sqrt{E}$ and independent of the delay time τ. The balls are smaller where the speed in phase space is smaller. The results are then consistent throughout the physically meaningful variation range for E and τ. We have worked with E between 6 and 16, τ between 4 and 6, and with a number $n_p\in[20,25]$ of sampled points in a typical time T_0. In this way, the embedding window $E\tau$ spanned a time interval corresponding to one to three fundamental periods T_0. A higher sampling rate increases the accuracy in the localization of the return. More important, however, is the total length of the time series which, in our case, was $N\approx 10^6$. With such a high number of data, we could observe many returns around the same periodic orbit. Once a close return point $\mathbf{x}_{i+n}$ is found, so that the distance $d(\mathbf{x}_i,\mathbf{x}_{i+n})$ is smaller than ε_i, the index i is incremented by 1 and the new relative error $\rho_{i+1}=d(\mathbf{x}_{i+1},\mathbf{x}_{i+n+1})/\varepsilon_{i+1}$ is computed. The initial index i is increased as long as ρ keeps decreasing, in order to find the best approximation to the unstable periodic orbit. It is important to consider the *relative* error: this prevents accepting a return as a good approximation to an actually periodic orbit when it occurs with a small absolute error but in a densely crowded region of the attractor. Since the data are available with limited precision (2^{-12} for the NMR laser; see Sec. IV) and are affected by noise, we also set a lower cutoff $\varepsilon_0(E)$ to the ball radius, below which no return is accepted. This value has been chosen as $\varepsilon_0(E)=a_2 2^{-12}\sqrt{E}$ (where a_2 is an adjustable constant). Finally, a test on the curvature of the initial and final branch of the closing orbit is made. If they do not agree within a given tolerance, the orbit is rejected. In fact, with a proper choice of the parameters, the probability of missing a close return can be made very small with a consequent increase of the number of spurious returns: i.e., of seemingly closing orbits that do not correspond to real cycles. Comparison of the results in different embedding dimensions helps discarding these curves. Since several slightly different approximations to the same actual cycle are usually found, we chose the one which better satisfied the following characteristics: displaying the closest return (relatively to the local precision ε_i, where preference was given to large ε's because of a reduced influence of noise); having the smallest angle between initial and final portion of the curve; and showing an overall smoother (i.e., noiseless) aspect (Finardi, 1993). The great accuracy achieved in this way has proved very useful in our investigation of a heteroclinic crisis, to be illustrated in Sec. IV.D.

Knowledge of the periodic orbits can be used to obtain a symbolic encoding of the motion. Before this is discussed, we recall a few elementary notions from the theory of nonlinear dynamics that are propaedeutic to symbolic dynamics. In order to map continuous trajectories to symbolic sequences, time t is first discretized by introducing a Poincaré surface Σ and considering the successive intersections of the trajectory with it. Depending on the system and on Σ, the intersection points can be accepted only if Σ is crossed in a given direction. We first illustrate this point for the Lorenz system (Lorenz, 1963)

$$\begin{aligned}\dot{x}&=-\sigma(x-y) ,\\ \dot{y}&=-y+rx-xz ,\\ \dot{z}&=-bz+xy .\end{aligned} \tag{2}$$

A convenient choice in this case is $\Sigma=\{(x,z):\dot{x}=\sigma(y-x)=0,\ \ddot{x}\,\mathrm{sgn}(x)<0\}$ (Badii *et al.*, 1992). In fact, since the motion is bounded, the time derivative of any of the coordinates vanishes recurrently (at irregular intervals of time). Hence no intersection is lost, by requiring that $\dot{x}=0$. The second condition takes into account the overall direction of the flow (2) in phase space: the trajectory moves roughly clockwise when looked at in the (x,z) plane for large $|x|$. It is therefore meaningful to accept the intersections generated by downward motion for positive x and vice versa for negative x. In this way, the map

$$\mathbf{x}_{n+1}=\mathbf{F}(\mathbf{x}_n) , \tag{3}$$

induced on Σ by the continuous-time dynamics, shares the same symmetry as the complete flow ($\mathbf{x}$ denotes the position vector on Σ, n is the discrete time, and $\mathbf{F}:\Sigma\to\Sigma$ is a generally unknown nonlinear function). For example, the flow possesses unstable cycles with a left-right symmetric shape in x which yield an even number of pairwise symmetric intersection points on Σ. Moreover, it has pairs of cycles, each the mirror image of the other, which yield sets of intersection points with the same property. The former orbits are "even" and the latter "odd." This would not be satisfied if the second condition for Σ had been just $\ddot{x}<0$ or $\ddot{x}>0$, irrespective of the sign of x. The surface Σ must also be chosen in such a way that the orbits do not touch it tangentially. The transversality condition $(1,-1,0)\cdot(\dot{x},\dot{y},\dot{z})\neq 0$ in our case is satisfied everywhere for $x=y$ except at $x=0$ or at $z=r-1$. These two planes pass through the three fixed points of the system: however, the strange attractors do not come close to such points at typical parameter values. We studied system (2) in the "standard" case $(\sigma,r,b)=(10,28,8/3)$ and at $(10,28,1)$. In Fig. 1, we display a projection of the strange attractor for the second parameter set, indicating the direction of the motion with arrows. The Poincaré section is just the line $x=y$. In the standard case, a binary partition, defined by

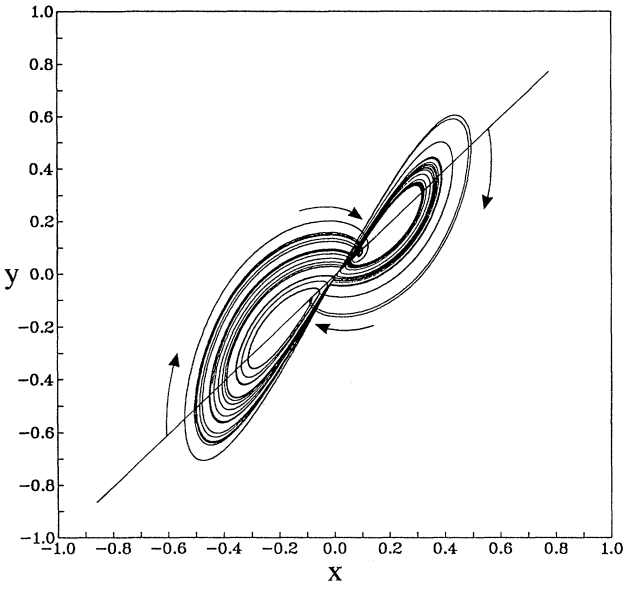

FIG. 1. Two-dimensional projection of the strange attractor of the Lorenz system (2) at $(\sigma,r,b)=(10,28,1)$. The line $x=y$ represents the intersection of the Poincaré surface with the (x,y) plane. The arrows indicate the direction of the flow.

$x=0$ in the (x,z) plane, suffices. When $b=1$, instead, the attractor in Σ consists of four pieces, as shown in Fig. 2.

Notice that careful consideration of symmetries and local direction of the flow must be made for each specific system under investigation. However, experimental low-dimensional attractors often have a simple (one-loop)

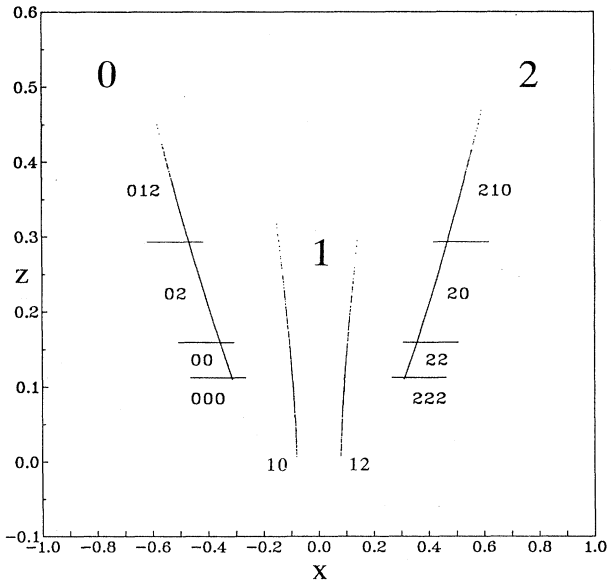

FIG. 2. Poincaré section of the flow shown in Fig. 1. The attractor consists of four branches. The large symbols (0,1,2) are the labels of the three elements of the generating partition (left, middle two, and right branches, respectively). The horizontal segments are the borders of a refinement of the partition, its elements being labeled by sequences of smaller-typeface symbols.

structure, and the choice of a Poincaré section is nearly straightforward.

In order to obtain a symbolic encoding of the motion on the attractors of a map $\mathbf{F}$, the space Σ is split into a finite number b of disjoint domains B_k, with $k\in A=\{0,\ldots,b-1\}$, covering the region where the asymptotic motion takes place (the invariant set). The collection $\mathcal{B}=\{B_k\}$ is hence a partition. Each orbit $\mathcal{O}=\{\mathbf{x}_1,\mathbf{x}_2,\ldots,\mathbf{x}_n\}$ is associated with a symbolic signal $\mathcal{S}=s_1s_2\ldots s_n$ consisting of the labels s_i of the domains B_{s_i} visited at times $i=1,2,\ldots,n$ (Alekseev and Yakobson, 1981). In turn, subdomains are indexed by concatenations $S=s_ks_l\ldots$ of symbols, all beginning with the label s_k of the parent set B_k: in this way, all points in element $B_{s_1s_2}$, for example, belong to B_{s_1} at time $i=1$ and will be mapped inside domain B_{s_2} at time $i=2$. All points $\mathbf{x}$ in B_s produce the same initial symbolic orbit S under the action of $\mathbf{F}$, before being spread over different domains B.

The first refinement $\mathcal{B}_1$ of $\mathcal{B}$ under $\mathbf{F}$ consists of the subsets $B_{s_i}\cap\mathbf{F}^{-1}(B_{s_j})$, for all $s_i,s_j\in A$ for which the intersection is not empty; its elements are labeled by pairs $\{s_i,s_j\}$ of symbols. Three-symbol sequences label the second refinement $\mathcal{B}_2$, and so on. In general, one has

$$\mathcal{B}_n\equiv\bigvee_{i=1}^{n}\mathbf{F}^{-i}\mathcal{B}=\mathcal{B}\vee\mathbf{F}^{-1}\mathcal{B}\vee\cdots\vee\mathbf{F}^{-n}\mathcal{B}\ , \tag{4}$$

where $\mathbf{F}^{-i}\mathcal{B}=\{\mathbf{F}^{-i}(B_0),\ldots,\mathbf{F}^{-i}(B_{b-1})\}$, and $\mathcal{B}\vee\mathcal{C}=\{B_i\cap C_j:\ 0\le i\le b-1, 0\le j\le c-1\}$ is called the *join* of two partitions $\mathcal{B}$ and $\mathcal{C}$ (having b and c elements, respectively). Successive refinements of the partition are represented by sequences S of increasing length (i.e., number of symbols) $n=|S|$.

The labeling is illustrated in Fig. 2, for the Lorenz system (2) at $b=1$ again. The attractor consists of four separate thin domains. However, owing to dynamical constraints, three symbols suffice for the encoding. The leftmost and rightmost branches are marked with 0 and 2, respectively. The middle two branches are grouped together under the heading 1. In fact, no matter which of them is visited, the next iteration specifies it uniquely: all points in the left region are mapped to branch 0, and those in the right region are mapped to branch 2. For this reason, the two domains are directly coded with a two-symbol sequence (10 and 12, respectively). Analogously, we indicate some subsets B_s, obtained by refining the partition, for sequence length $|S|\le 3$. All points in element 20, for example, are mapped to branch 0 in one iteration, those in 000 to element 00, first, and to either 02 or 012 at the next step.

The phase-space dynamics given by a map $\mathbf{F}$ is translated, in the space of all symbolic sequences $\mathcal{S}=\ldots,s_{-1}s_0s_1\ldots$ over the alphabet $\mathcal{A}$, into the left shift homeomorphism $\hat{\sigma}:\hat{\sigma}(\mathcal{S})_i=s_{i+1}$ (where s_i is the ith symbol in $\mathcal{S}$). The set $\mathcal{L}$ of all sequences S generated by the system is called the language. The study of the symbolic dynamical system $(\Sigma_L,\hat{\sigma})$, where Σ_L is the set of all

infinite sequences compatible with $\mathcal{L}$, is equivalent to the study of the map **F** if the partition $\mathcal{B}$ is generating, that is, if every infinitely long symbolic sequence corresponds to a unique initial condition **x** (Alekseev and Yakobson, 1981). Partitions of this type are refined indefinitely by the dynamics, according to Eq. (4). They also yield the supremum of the Kolmogorov-Sinai entropy over all possible partitions (Cornfield *et al.*, 1982; Eckmann and Ruelle, 1985; Guckenheimer and Holmes, 1986). Even if the trajectory of the map is chaotic, a carelessly chosen partition might yield a periodic symbolic sequence, with a great loss of information on the system.

Generating partitions can be constructed systematically in hyperbolic systems (Guckenheimer and Holmes, 1986), for which stable and unstable manifolds intersect transversally at each point (Eckmann and Ruelle, 1985). However, it is not known how to identify a generating partition for "generic," nonhyperbolic dynamics, which is characterized by the occurrence of tangencies between stable and unstable manifolds or by the lack of exponential repulsion in certain regions of the space (corresponding to the negativity of all Lyapunov exponents computed over a finite portion of the trajectory). Nonhyperbolic motion is considered to be generic in real systems. Notwithstanding this, the existence of a strange attractor in such a case has been questioned for a long time: in fact, there is an infinity of stable periodic points arbitrarily close to the invariant curves of a nonhyperbolic map (Newhouse, 1974). The proof that this is not incompatible with the existence of a strange attractor has been given by Benedicks and Carleson (1991).

In the special case of two-dimensional maps with homoclinic tangencies, like Hénon's (Hénon, 1976), it has been conjectured that a curve passing through the "primary" tangency points would yield the correct symbolic dynamics (Grassberger and Kantz, 1985; Grassberger *et al.*, 1990). Yet, no rigorous result has so far been established; and a practical implementation of this idea is itself rather problematic, since a precise definition of "primary" tangencies is lacking (at these points the curvature of both stable and unstable manifolds must be "small"). Moreover, even when some can be localized, the finiteness of their number and the positions at which they occur may prevent a "simple" joining curve from being found (Giovannini and Politi, 1991, 1992). No analogous procedure exists for higher-dimensional attractors.

Another method is suggested by the simple observation that in order for a partition to be generating it must attribute to all periodic points (stable or unstable) a different symbolic label: in fact, a periodic orbit γ is a special, infinitely long orbit. A partition $\mathcal{B}$ that fulfills this fundamental requirement constitutes a good approximation to a generating one. The accuracy is limited by the maximum cycle length T that can be observed either experimentally or numerically and, possibly, by the nonhyperbolicity of the map **F**. In fact, the set of unstable periodic points of **F** has been proved to be dense on the attractor only in the hyperbolic case (Eckmann and Ruelle, 1985; Auerbach *et al.*, 1987). Hence separating just the unstable periodic orbits may not be asymptotically sufficient, in general.

It is well known that the minimum number b of symbols necessary for the encoding is lower-bounded by the exponential e^{K_0} of the topological entropy K_0 (Adler *et al.*, 1965) which satisfies the asymptotic relation

$$N(T) \sim \frac{e^{K_0 T}}{K_0 T} \quad \text{for } T \to \infty \ , \tag{5}$$

where $N(T)$ is the number of closed (i.e., periodic) orbits with period less than T (Pollicott, 1991). Hence the identification of the unstable cycles of the system, up to some maximum length T, allows one to estimate the cardinality b of the partition. This idea was first applied to a few planar maps (Badii, 1989b, 1990). In particular, for the Hénon map (Hénon, 1976), we assigned a first trial partition (defined by $y=0$) and checked it against the periodic points of increasing order n. The partition was modified when it failed to distinguish symbolically two different periodic points (the change was in the form of a little step). The iteration of this procedure, restarting from $n=1$ after each modification, finally led to a piecewise constant curve which could separate all points up to order $n=23$. The symbolic encoding was in perfect agreement with that obtained in Grassberger and Kantz (1985) and Grassberger *et al.* (1990). This procedure, which has been successfully applied to the Lorenz system and other flows (Finardi, 1993), is particularly convenient when dealing with experimental time series affected by noise and embedded in a relatively high-dimensional space. If the length N of the time series is large and, *a fortiori*, if the data have been processed with some noise-reduction algorithm (Grassberger *et al.*, 1993), the unstable periodic orbits can be located with good precision. For all maps and flows that we studied numerically, the Kolmogorov-Sinai entropy (Cornfeld *et al.*, 1982) as computed from the symbolic dynamics (see Sec. IV) agreed with alternative estimates based on phase-space methods or Lyapunov exponents (Grassberger *et al.*, 1988). Application to experimental time series will be discussed in Sec. IV.

Notice that the partition given in terms of periodic points can be easily specified in any dimension and that it is not restricted to planar maps. In fact, one may first assign a symbolic label to the $N(n)$ periodic points up to some order n (e.g., 1, 01, 10, for $n=2$), which are taken as a reference for the next step in the procedure. All those with the same initial symbol $s \in \mathcal{A}$ define a set C_s. For any point **x** of the chaotic trajectory, one need simply find the nearest neighbor **y** among the $N(n)$ reference points: then, **x** is assigned the same symbol s as the set C_s containing **y**. The space is thus tiled according to a Voronoi partition $\mathcal{B}=\{B_0, \ldots, B_{b-1}\}$, each element B_s containing the reference points of C_s and their nearest neighbors (i.e., all points that are closer to C_s than to any

other $C_{s'}$ with $s \neq s'$). The procedure can be rendered automatic: having classified the $N(n)$ points with periods $i \leq n$, one labels the period-$(n+1)$ points according to the neighborhoods at level n and obtains the next partition. However, a few consistency checks are still necessary, to avoid two different period-$(n+1)$ points being attributed the same symbolic sequence $S = s_1 s_2 \ldots s_{n+1}$. It may be necessary to readjust the partition (through a redefinition of the reference points $\mathbf{y}$) during the scanning of the order-$(n+1)$ points and not just at the end of it.

III. THE NMR LASER AND ITS MATHEMATICAL MODEL

The simplest form of laser dynamics arises from the interaction between a single-mode field and a medium with a homogeneous gain line in which a population inversion is induced by a suitable pumping process (Sargent *et al.*, 1974). The laser was one of the first experimental systems to be studied in the chaotic regime (Arecchi *et al.*, 1982; Abraham *et al.*, 1985). At resonance, its mathematical description is essentially equivalent to the Lorenz model (Haken, 1975), which suggested the possible occurrence of chaotic instabilities well before the first experiments were undertaken. In fact, early evidence of aperiodic behavior was already given in Grasiuk and Oraevskij (1964). Since then, chaotic laser dynamics has been studied in a large number of systems under different experimental arrangements (Boyd *et al.*, 1986).

A laser consists of two main parts: the radiating particles (atoms, molecules, electrons, nuclei) and the radiation field produced by them. An external pump yields the population inversion where the higher energy states are more strongly populated than the lower ones. A resonant structure (cavity), which encloses the particles, provides the feedback for the radiation field, thus causing the coherent excitation and radiation of the particles. Qualitatively similar behavior to that of optical devices can be obtained in the nuclear-magnetic-resonance (NMR) laser, which is able to provide radio-wave amplification by stimulated emission of radiation (Bösiger *et al.*, 1977). The lasing "particles" in this system are represented by the nuclear spins of the ^{27}Al in a ruby ($Al_2O_3:Cr^{3+}$) crystal. The radiation field is a magnetic radio-frequency (rf) field sustained by a tuned NMR coil which forms the cavity of the laser (see Fig. 3). Spin inversion beyond the first laser threshold is obtained by means of dynamic nuclear polarization (DNP) at the temperature of 4.2 K. DNP is achieved by shining microwaves at Cr^{3+}, thus causing electronic transitions that pump the nuclear spins to the lasing state. The ruby NMR laser typically operates at the central NMR frequency $\nu_a = 12.3$ MHz of ^{27}Al in a static magnetic field $B_0 = 1.1$ T. The NMR cavity is usually tuned to ν_a, so that the system acts as a tuned, single mode, homogeneously broadened, unidirectional laser.

The NMR laser field induces a voltage in the receiver coil L which can be tapped at the tuning capacitor C. Thus the signal is the voltage $V(t)$ across C which oscillates at ν_a. Since laser chaos primarily appears as irregular variations of the amplitude of V, the rf laser signal is demodulated and only its envelope $v(t)$ is recorded. We call $v(t)$ the laser output.

Since the first investigations of its chaotic behavior (Meier *et al.*, 1982), the NMR laser has distinguished itself from optical devices because of the high accuracy and good reproducibility of the measurements. Moreover, a set of dynamical equations could be derived from fundamental laws of physics where all relevant parameters are under experimental control, a prerequisite for the comparison between theory and experiment. In particular, it has been studied in a number of different setups: as a free-running laser (Bösiger *et al.*, 1977, 1979), as a small signal detector (Derighetti *et al.*, 1985), with a parametric modulation (Brun *et al.*, 1983, 1984, 1985; Brun, 1991), with an injected signal (Brun *et al.*, 1985,

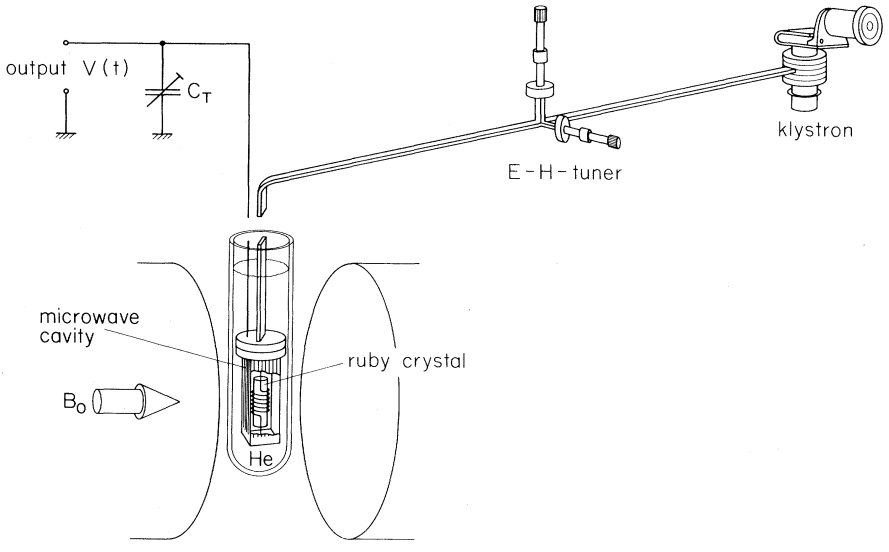

FIG. 3. Schematic representation of the experimental setup for the NMR laser.

1986), with phase-locked feedback (Holzner *et al.*, 1987), and with delayed feedback.

The early work was interpreted with a conventional Bloch-type laser (CBL) model (Bösiger *et al.*, 1978; Brun *et al.*, 1985), the analog of the optical Maxwell-Bloch equations. However, that model could at most only qualitatively describe the observed behavior. In particular, the CBL model was unable to account for the relaxation mechanisms of the system. Therefore we focused our work in recent years on the search for more accurate laser equations. A systematic investigation of the transients after Q switching suggested that a small nonlinear correction for the damping of the phase memory (transverse relaxation) of the spins was most likely the key to improved Bloch-type equations. The inclusion of such a term in the CBL model was a breakthrough: the resulting extended Bloch-type laser (EBL) equations (Flepp *et al.*, 1990; Flepp, 1991) have been shown to represent a very accurate mathematical basis for the interpretation of NMR laser experiments. The most striking verification of their suitability was obtained in a detailed periodic orbit analysis of the system (Flepp *et al.*, 1991; Finardi, 1993), which will be reviewed in the next section.

It must be remarked that a general theory for the NMR laser has not yet been formulated and that the available models constitute just phenomenological approximations. They consist of Bloch's equations, describing the classical collective dynamics of the ^{27}Al spins, complemented by Kirchhoff's rules for the electronic circuitry that provides the "laser field." The nuclear-spin relaxation is treated heuristically by introducing suitable relaxation rates. The dynamic nuclear polarization is finally expressed by a pumping rate and a pumping level. The resulting model describes the behavior of macroscopic variables that represent an average of the exceedingly complicated interactions among the nuclear and electronic spins and of their coupling to the crystal electric field and to the external microwave field which ultimately pumps ^{27}Al. Spin-spin interactions mediate the energy transfer from the lasing spins to both the pumping field and the crystal lattice. Spin-spin interactions are also responsible for the irreversible dephasing of the radiating ^{27}Al nuclei.

A. Spin dynamical aspects of ruby

The activity of the ruby NMR laser strongly depends on the coupling of the nuclear ^{27}Al and electronic Cr^{3+} spins with the magnetic and electric fields and among themselves. The Hamiltonian of the combined nuclear and electronic spin system can be split into terms that represent magnetic (Zeeman), electric (crystal-field), and spin-spin (dipole-dipole) interactions. There appear mutually commuting and noncommuting terms, $\mathcal{H}_i$ and $\mathcal{H}_{ik}$, respectively. Each of the commuting operators characterizes an energy reservoir with many degrees of freedom. Since the crystal-field effects are small compared with the Zeeman interaction, we loosely speak of the nuclear and electronic Zeeman reservoirs coupled to the dipole-dipole interaction reservoir. In thermal equilibrium, a spin temperature θ_i may be assigned to each of these subsystems.

The noncommuting operators describe internal couplings (spin-spin, spin-lattice) or interactions with time-dependent external fields and are treated as perturbations. They are responsible for the energy flow between the reservoirs. The internal couplings tend to equalize the temperatures with time constants τ_{ik} (dephasing or relaxation and cross-relaxation times): they reflect dissipation. In contrast, the interactions with coherent radiation fields tend to counteract the overall thermal equilibrium. In fact, they may produce spin order, for example, by contributing to the pumping of certain spin states or by synchronizing the phases of otherwise randomly oriented single spins.

The lasing "particles" in the NMR laser are the magnetic dipole moments $\boldsymbol{\mu}$ of the ^{27}Al nuclei in ruby. They interact with the static magnetic field $\mathbf{B}_0$ and with the (transverse) radiation field $\mathbf{B}_t(t)$ by the magnetic dipole interaction $\mathcal{H}=-\boldsymbol{\mu}\cdot\mathbf{B}$, where $\mathbf{B}=\mathbf{B}_0+\mathbf{B}_t$. The ^{27}Al nucleus has spin 5/2, a gyromagnetic ratio $g=6.97\times10^7$ $s^{-1}T^{-1}$ (we use the symbol g instead of γ, which is reserved for relaxation rates; in doing so, we follow the notation of quantum optics), and an electric quadrupole moment. In ruby, ^{27}Al occupies equivalent sites. The nuclear Zeeman levels $E_m=-mg\hbar B_0$, with $m\in\{\pm5/2, \pm3/2, \pm1/2\}$, are thus shifted in a unique way by the quadrupole interaction of ^{27}Al with the crystal electric field. This amounts to five generally different resonance frequencies $\omega_a^{(i)}$ for the $\Delta m=\pm1$ spin-flip transitions. Since the LC circuit that forms the laser cavity has only one resonance frequency, $\omega_c=1/\sqrt{LC}$, the NMR laser has at most five modes. Single-mode activity is possible when the coil is tuned to a selected NMR transition. In this case, the spin inversion should not exceed the threshold beyond which multimode excitation occurs. Unless otherwise stated, we restrict ourselves to the single-mode activity of the strongest $(1/2,-1/2)$ NMR transition with frequency $\omega_a=gB_0$: the central NMR mode.

The Cr^{3+} impurity ions replacing the ^{27}Al ions in ruby, on the one hand, shorten the spin-lattice relaxation time T_1 for ^{27}Al while, on the other, they provide a mechanism to polarize the spins either positively or negatively with respect to the direction of the static magnetic field $\mathbf{B}_0$. The experimental optimum for short relaxation and strong polarization was found in a specimen cut from a single crystal with a Cr^{3+} concentration of nominally 0.02%.

The efficiency of the dynamic nuclear polarization technique has been tested by comparing enhanced NMR signals with those taken at the lattice temperature θ_L. The largest enhancement factor (about 400), corresponding to a nuclear-spin polarization of approximately 17%, has been observed at $\theta_L=1.9$ K for a crystal orientation of about 61° between the c axis and $\mathbf{B}_0$. This is the standard orientation with which all our experiments have

been performed. At this angle, the two strongest electron-spin resonance (ESR) transitions coincide, and the laser behavior is optimal.

In order to research the laser threshold, the nuclear spins have to be oriented in the direction opposite to $\mathbf{B}_0$ with an overall negative polarization of the order of 10%, which corresponds to a negative spin temperature of some millikelvins. This condition is easily met at the lattice temperature of liquid He when microwaves of frequency ω are supplied to the sample with ω near an ESR transition frequency ω_e of the Cr^{3+} impurity ions. Setting ω slightly above ω_e then leads to the required low, negative spin temperature. Microwave energy is thereby absorbed and delivered to the Cr^{3+}-Cr^{3+} spin-spin system. Its spin temperature θ_{ss} rises to negative values; spin-spin order is thus greatly enhanced. Furthermore, since the ^{27}Al Zeeman splitting is smaller than the Cr^{3+} linewidth, the coupling of nuclear and electronic spins allows now the exchange of energy between the electronic spin-spin and the nuclear Zeeman system. The latter is therefore effectively pumped by DNP to a negative spin temperature.

B. Conventional Bloch equations for the NMR laser

In the single-mode NMR laser the active ^{27}Al spins may be considered as members of a two-level system to which an averaged Bloch vector $\mathbf{M}=(M_x,M_y,M_z)$ can be assigned. The three macroscopic variables (M_x,M_y,M_z) are the components of the nuclear magnetization $\mathbf{M}$ characterizing the active spins, referred to a coordinate system that is fixed in the laboratory, the directions x and z being parallel to the axis of the NMR coil and to $\mathbf{B}_0$, respectively. The vector $\mathbf{M}_t=(M_x,M_y,0)$ represents the transverse component of $\mathbf{M}$ which, in the radiating state, precesses about $\mathbf{B}_0$. The vector $(0,0,M_z)$ is called the longitudinal component of $\mathbf{M}$. Its value is proportional to the population difference of the two Zeeman levels that are engaged in the radiative process. Those nuclear Zeeman levels that are not involved in the single-mode behavior play an important role for the storage of the nuclear Zeeman energy that can be delivered to the active spins. These inactive spins form a separate energy reservoir whose content is also controlled by the DNP pump. It acts as a buffer, thereby drastically reducing the fluctuations of the microwave pump. For our purpose, we can lump the microwave pump and the reservoir spins together. Thus we form an effective DNP pump system to which we assign an operationally defined pump magnetization M_e. With this, we imply that the effective DNP pump tends to equalize M_z and M_e. Two further macroscopic variables of the NMR laser are amplitude and phase of the coherent radiation field $\mathbf{B}(t)$, the former being proportional to the current $I(t)$ in the NMR coil.

The dynamic equations for the macroscopic variables of the NMR laser are the analog of the Maxwell-Bloch equations of quantum optics. In order to obtain them, we consider the oscillating radiation field $\mathbf{B}(t)$ acting on the nuclear spins. We retain only those components that rotate in the same sense as the precessing spins and introduce a reference frame (u,v,z) that similarly rotates around $\mathbf{B}_0$ with frequency ω. Accordingly, $\Delta\omega_a=\omega_a-\omega$ is called the NMR detuning and $\Delta\omega_c=\omega_c-\omega$ represents the coil or cavity detuning. Although ω may be freely chosen, it is convenient to set $\omega=\omega_a=\omega_c$ for the tuned, free-running NMR laser. In the case of an externally driven NMR laser, we may set $\omega=\omega_d$, with ω_d the frequency of the injected field. The phase of the rotating frame is still free: we fix it by letting the u and x axes coincide at $t=0$. Hence we assume that the five macroscopic variables (M_u,M_v,M_z) and (B_u,B_v) of the single-mode NMR system obey, in the rotating-frame representation, the conventional Bloch equations

$$\begin{aligned}
\dot{M}_u &= -\gamma_\perp M_u + \Delta\omega_a M_v - s^2 g B_v M_z \ , \\
\dot{M}_v &= -\gamma_\perp M_v - \Delta\omega_a M_u + s^2 g B_u M_z \ , \\
\dot{M}_z &= -\gamma_\parallel (M_z - M_e) + g(B_v M_u - B_u M_v) \ ,
\end{aligned} \tag{6}$$

where $\gamma_\perp$ and $\gamma_\parallel$ are suitable damping constants (to be discussed below) and s is a spin factor that has been introduced to account for the fictitious spin-1/2 nature of the ruby laser when it is interpreted as a two-level system. Indeed, only two of the $2I+1$ levels of the real system are relevant. For the special case $I=1/2$, we have $s=1$. In general, s must be calculated from quantum-mechanical rules (Abragam, 1961). For the single-mode ruby laser with ^{27}Al as a spin-5/2 system, s^2 takes the values 9, 8, or 5, depending on the chosen NMR mode $(1/2,-1/2)$, $(1/2,3/2)$, or $(3/2,5/2)$, respectively. For our standard NMR mode, we have $s=3$.

The two characteristic time constants $\gamma_\perp=1/T_2$ and $\gamma_\parallel=1/T_e$ govern the relaxation of the three macroscopic variables (M_x,M_y,M_z). The former characterizes the decay of the transverse nuclear magnetization M_t which can be seen as a dephasing of the collective motion of the nuclear spins, caused by spin-spin interactions. The time constant T_e can be attributed to the effective DNP pump system (Brun *et al.*, 1985), since interactions among the nuclear ^{27}Al and the electronic Cr^{3+} spins in ruby contribute to transfer the Zeeman energy among the spins: in particular, from the effective DNP pump system to the lasing spins of ^{27}Al. Thus T_e represents the pump time constant associated with the relaxation of M_z toward the constant pumping level M_e.

It must be stressed that this drastic simplification of the complicated spin and DNP pump dynamics in ruby is only justified for the special operating conditions of the NMR laser if the variations of M_z are small; typically, they are less than a few percent. In that situation, the pumping conditions remain stable and M_e is approximately constant. Hence the contribution of the slow spin-lattice relaxation and of the dynamic nuclear polarization to the decay process can be neglected. T_e then

plays the role of a Bloch-type longitudinal relaxation time.

In order to complete the laser equations, the components $B_u(t)$ and $B_v(t)$ of the self-induced transverse radiation field $\mathbf{B}_t(t)$ must be expressed in terms of the parameters of the NMR LC circuit. To this end, we observe that

$$B_t(t)=\frac{\mu_0 NI(t)}{l} , \tag{7}$$

where $I(t)$ is the current flowing in the NMR coil which has length l and N windings. The relationship between the induced emf $V_{\rm ind}$ and the current I is given by Kirchhoff's law:

$$\ddot{I}+\frac{\omega_c}{Q}\dot{I}+\omega_c^2 I=\frac{1}{L}\dot{V}_{\rm ind} , \tag{8}$$

where $Q=R_p/\omega_c L$ is the quality factor of the coil and R_p is the effective Ohmic parallel resistance. From Faraday's induction law we further have

$$V_{\rm ind}=-\mu_0\eta SN\frac{d}{dt}(M_u\cos\omega t+M_v\sin\omega t) , \tag{9}$$

under the assumption that the nuclear magnetization inside the coil is homogeneous. The parameters η and S are the filling factor and the cross section of the NMR coil, respectively.

By substituting Eqs. (9) and (7) into Eq. (8) and considering that our system satisfies the conditions

$$\dot{M}_t \ll \omega M_t, \quad \max\{|\Delta\omega_c|,|\Delta\omega_a|\} \ll \min\{\omega_a,\omega_c,\omega\} ,$$

$$\omega_c^2 \gg \frac{\omega_c}{Q} \gg 1 ,$$

the second derivative in Eq. (8) can be dropped. The laser field equations thus become

$$\begin{aligned}\dot{B}_u&=-\kappa B_u+\Delta\omega_c B_v-\chi M_v ,\\ \dot{B}_v&=-\kappa B_v-\Delta\omega_c B_u+\chi M_u ,\end{aligned} \tag{10}$$

where the field decay constant κ and the coupling constant

$$\chi=\frac{\mu_0\eta Q\kappa}{2} \tag{11}$$

have been introduced. The former equals $1/T_R$, where T_R is the ringing time of the LC circuit. Hence $\kappa=\omega_c/2Q$. The expression for χ has been obtained from the well-known relation $L=\mu_0 N^2 S/l$.

Equations (6) and (10) together constitute the conventional Bloch laser model. In the case of single-mode operation involving the levels $(-1/2,1/2)$ with perfect tuning $\Delta\omega_c=\Delta\omega_a=0$, they read

$$\begin{aligned}\dot{M}_u&=-\gamma_\perp M_u-9gM_z B_v ,\\ \dot{M}_v&=-\gamma_\perp M_v+9gM_z B_u ,\\ \dot{M}_z&=-\gamma_\parallel(M_z-M_e)+g(B_v M_u-B_u M_v) ,\\ \dot{B}_u&=-\kappa B_u-\chi M_v ,\\ \dot{B}_v&=-\kappa B_v+\chi M_u .\end{aligned} \tag{12}$$

C. Extended Bloch-type laser equations

The CBL equations (12) describe the behavior of both amplitude and phase of the transverse magnetization $\mathbf{M}_t$ and of the field $\mathbf{B}_t$ through their (u,v) components. Hence, in order to exploit them completely, it would be necessary to utilize a phase-sensitive detection scheme. In this way, one could observe, for example, amplitude and phase chaos. The latter is a phenomenon of great potential interest in itself which, however, causes extreme experimental difficulties because of long-time stability requirements for the reference phase.

In a more modest approach, we restricted therefore our investigation to the amplitude dynamics for which the possible phase fluctuations are of minor importance. In that case, the CBL model (12) can be reduced to a set of only three differential equations by choosing a convenient phase of the rotating frame. For this purpose, we retain only the variables M_v, M_z, and B_u (notice that the discarded M_u and B_v behave exactly as $-M_v$ and B_u, respectively, apart from the initial condition) to obtain

$$\begin{aligned}\dot{M}_v&=-\gamma_\perp M_v+9gM_z B_u ,\\ \dot{M}_z&=-\gamma_\parallel(M_z-M_e)-gM_v B_u ,\\ \dot{B}_u&=-\kappa B_u-\chi M_v .\end{aligned} \tag{13}$$

This system can be further written in the form of the Lorenz equations (2) by introducing the dimensionless variables

$$x=\frac{3g}{\gamma_\perp}B_u, \quad y=-\frac{3g\chi}{\kappa\gamma_\perp}M_v, \quad z=\frac{9g\chi}{\kappa\gamma_\perp}(M_z-M_e) . \tag{14}$$

The derivatives are taken with respect to the dimensionless time $\tau=t\gamma_\perp$. The parameters

$$\sigma=\kappa\gamma_\perp^{-1}, \quad r=\frac{9g\chi}{\kappa\gamma_\perp}|M_e|, \quad \text{and } b=\gamma_\parallel\gamma_\perp^{-1} \tag{15}$$

have the values $\sigma=4.875$, $r=1.807$, and $b=2\times10^{-4}$ (see Table I), which do not allow for any chaotic behavior. The system always relaxes to one of the two asymptotically stable fixed points

$$x=y=x_0=\pm\sqrt{b(r-1)}, \quad z=z_0=r-1 \tag{16}$$

with a damping constant $\gamma_{\rm rel}=b/2$ and a frequency $\omega_{\rm rel}=\sqrt{2x_0^2-b^2/4}=1.797\times10^{-2}$. In physical units,

they correspond to $\gamma_{\parallel}/2\approx 2.4\ \mathrm{s}^{-1}$ and to $\nu_{\mathrm{rel}}\approx 67.7$ Hz.

Early investigations (Brun *et al.*, 1985) have shown that the CBL model reproduces only qualitatively the behavior of the real system. Therefore, we reconsidered critically the various steps of its derivation. The crucial modification has been suggested by the observation of the laser transients towards the stable state after an external perturbation (Flepp, 1991). Indeed, Eqs. (6) account for just the exponential decay of the transverse nuclear magnetization $\mathbf{M}_t$ in the absence of the radiation field (free-induction decay or FID) with the phenomenological relaxation time $T_2=1/\gamma_{\perp}$. Although deviations from this simple behavior are common in solids with complex spin-spin and spin-lattice interactions, the single ruby crystal of the NMR laser at standard orientation exhibits a FID that comes close to an exponential decay when the radiative feedback is small. However, the CBL model does not appropriately describe transients occurring after a perturbation of the free-running-laser conditions. Since this appears to be the effect of a nonlinearity in the relaxation mechanism, we assume the following extended Bloch equation to hold for the FID of the ruby NMR laser:

$$\dot{M}_t=-\gamma_{\perp}\left[1+\frac{\alpha}{s}M_t\right]M_t\ , \tag{17}$$

with $M_t=|\mathbf{M}_t|$. Here, α is an *a priori* unknown fit parameter that can be considered as the coefficient of the lowest-order term in a Taylor expansion modeling a nonexponential spin dephasing. Although the correction term $\alpha M_t/s$ is of the order of 10^{-3}, the new relaxation rule dramatically improves the accuracy of the model. It has to be remarked that there exists at present no quantitative theory that could explain assumption (17). Hence corrections of this type remain heuristic for the time being (since $\mathbf{M}_t$ is closely related to $\mathbf{B}_t$, the new contribution might be interpreted as a dephasing effect caused by the radiation field).

The complete extended Bloch laser model (EBL), in the rescaled variables (14), takes the form

$$\begin{aligned}\dot{x}&=-\sigma(x-y)\ ,\\ \dot{y}&=-y(1+ay)+rx-xz\ ,\\ \dot{z}&=-bz+xy\ ,\end{aligned} \tag{18}$$

where

$$a=\frac{\alpha\kappa\gamma_{\perp}}{9g\chi}\approx 0.262\ . \tag{19}$$

Finally, by further introducing the variables

$$X=x/x_0,\quad Y=y/x_0,\quad Z=(z-z_0)/x_0 \tag{20}$$

and the new time $\tau'=\tau x_0$, we obtain

$$\begin{aligned}\dot{X}&=-\sigma'(X-Y)\ ,\\ \dot{Y}&=-Y(c+aY)+X(c-Z)\ ,\\ \dot{Z}&=-\beta Z-1+XY\ ,\end{aligned} \tag{21}$$

where $\sigma'=\sigma/x_0\approx 384\gg 1$, $c=1/x_0\approx 79$, and $\beta=b/x_0\approx 1.57\times 10^{-2}$. The values of X, Y, and $|Z|$ remain in the range [0,3] under all conditions, including chaotic behavior (to be discussed later). Hence the term aY is clearly small with respect to c. Moreover, the large value of σ' renders the adiabatic elimination of X possible, yielding

$$\begin{aligned}\dot{Y}&=-Y(aY+Z)\ ,\\ \dot{Z}&=-\beta Z-1+Y^2\ .\end{aligned} \tag{22}$$

Notice that the Y variable never changes sign, since its derivative $\dot{Y}$ is proportional to Y itself. This is in agreement with the fact that Y represents the modulus of the

TABLE I. Experimentally determined NMR laser parameters for standard running conditions. The numerical values are used to calculate the system parameters of the EBL model.

NMR laser parameters			
Gyromagnetic ratio	g	6.97×10^{7}	[1/sT]
Lattice temperature	T	4.2	[K]
Quality factor	Q	330	
Static NMR field	B_0	1.109	[T]
Laser frequency	ν_a	12.3×10^{6}	[Hz]
Pump magnetization	M_e	-0.78	[A/m]
Threshold magnetization	M_k	0.436	[A/m]
Longitudinal pump rate	$\gamma_{\parallel}$	4.76	[1/s]
Transverse decay rate	$\gamma_{\perp}$	2.38×10^{4}	[1/s]
EBL dephasing coefficient	α	0.607	[m/A]
Filling factor	η	0.42	
Coupling constant	χ	10.19	[Tm/As]
LC ringing constant	κ	1.17×10^{5}	[1/s]
Relaxation frequency	ν_{rel}	65.5 ± 0.5	[Hz]
Relaxation rate	γ_{rel}	2.4 ± 0.1	[1/s]
Bandwidth	$\Delta\nu$	37.2×10^{3}	[Hz]
Length of the wire	l	1.30×10^{-2}	[m]
Radius of the wire	R	0.17×10^{-3}	[m]
Number of windings	N	30	

transverse magnetization vector $\mathbf{M}_t$. Clearly, the most suitable variable for this model is then $W=\ln Y$.

D. Chaotic laser behavior

The previous discussion shows that the onset of chaos in the NMR laser is prevented within the accessible parameter space of the system. In fact, the system can be described by a set of only two ordinary differential equations. However, if an external driving is applied, for example, in the form of a sinusoidal modulation of a system parameter, the additional degree of freedom makes chaotic behavior possible. Experimentally, this has been realized by varying a parameter p in time according to $p(t)=p_0(1+A\cos\omega_m t)$, where the modulation frequency $\nu_m=\omega_m/2\pi$ is chosen in the range [20,150] Hz, i.e., close to the relaxation frequency $\nu_{\rm rel}\approx 67.7$ Hz of the free-running laser. The response of the driven laser has been studied by acting on various parameters: DNP pumping strength, cavity detuning, NMR linewidth $\gamma_\perp$, and quality factor Q. In particular, the latter two offer favorable operating conditions requiring relatively weak forcing signals, with the amplitude A lying in the range [0,0.03]. The $\gamma_\perp$ modulation is obtained by superimposing an oscillating field gradient on the homogeneous field B_0. A detailed account of the associated phenomenology can be found in Ravani *et al.*, (1988) and Flepp (1991). In this work, we survey experiments conducted with the Q-modulated NMR laser. This type of forcing is accomplished by varying the resistance of the NMR circuit. The first equation in EBL model (18) must therefore be modified to

$$\dot{x}=-\sigma(x/f(t)-y)\ , \tag{23}$$

where $f(t)=1+A\cos\omega t$, and $\omega=\omega_m/\gamma_\perp$ is the modulation frequency, rescaled as explained above. The adiabatic elimination now yields $X=Yf(t)$, in transformed system (21). In the next section, we display the phase diagram of this system to illustrate the types of chaotic behavior occurring under the usual experimental conditions.

IV. MODEL-EXPERIMENT COMPARISON

In order to test the efficiency of the two available models for the NMR laser, it is necessary to have good knowledge and control of the system parameters. Fortunately, the NMR laser belongs to the rare, nontrivial many-body systems where all relevant parameters can be determined with good accuracy. Some of them may be measured directly (Q factor, laser frequency); the others (filling factor, damping constants, etc.) can be obtained indirectly, either by fitting the laser response after a suitable perturbation, or by performing appropriate supplementary NMR measurements. Table I displays the parameter values that characterize the ruby NMR laser at the temperature of liquid helium. Owing to the reliability of these measurements, any discrepancy between the CBL and EBL models that lies within the experimental resolution is to be attributed to qualitative differences in the dynamics.

A. Basic test of the extended Bloch-type laser model

We first discuss the effect of the inclusion of the new parameter α in the EBL model on the relaxation of the transverse magnetization. The most direct estimate of α is made by inducing a transient toward the steady state $\mathbf{M}_t^s=(M_v^s,M_z^s)$ [corresponding to $Y=Y_1\approx 1-a\beta/2$, $Z=Z_1=-aY_1$ for the rescaled system (22)] by means of a controlled Q-switching technique. The laser is first allowed to relax to $\mathbf{M}_t^s$ with an initial quality factor Q. Then, at some later time, the quality factor is abruptly lowered to a value Q_e ("Q quenching"), which is kept constant for a time T_q until the original value Q is restored. The output voltage $v(t)\propto M_v(t)$ is recorded thereafter.

If the laser action is completely quenched in the interval T_q (i.e., $Y\approx 0$), the subsequent laser pulses, followed by the relaxation to the fixed point $\mathbf{M}_t^s$, will be triggered

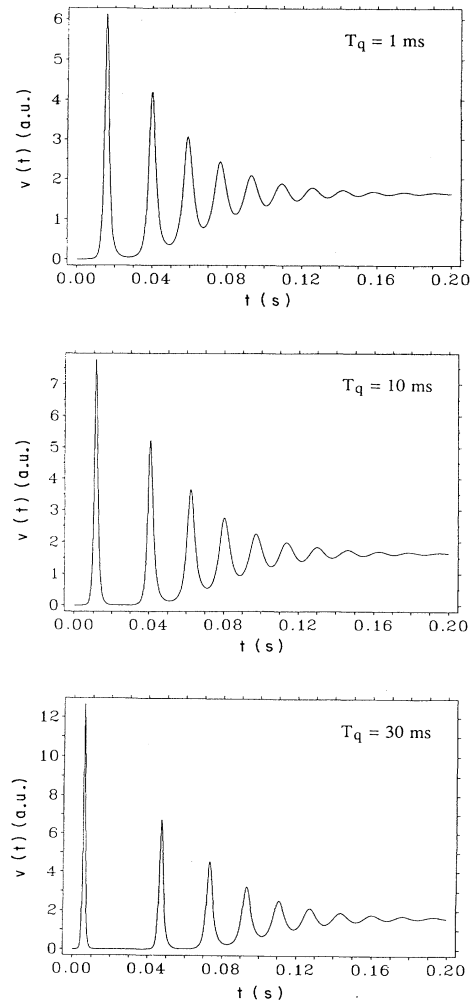

FIG. 4. Demodulated laser output $v(t)$ vs t after Q quenching, for three different quenching times T_q.

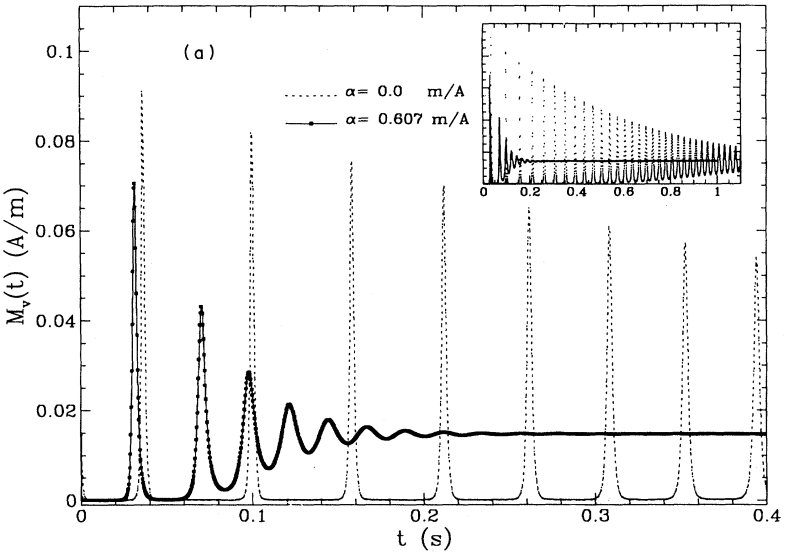

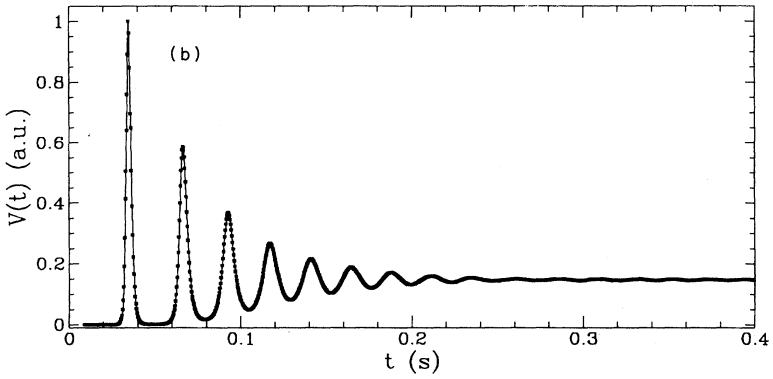

FIG. 5. Laser transients as obtained from the numerical simulations (a) and from the experiment (b), after Q quenching. The quenching time was $T_q=2$ ms. In (a) the outcome of the EBL model (solid line, $\alpha=0.607$) is compared with that of the CBL model (dashed line, $\alpha=0$). Notice the striking similarity between EBL result and experiment.

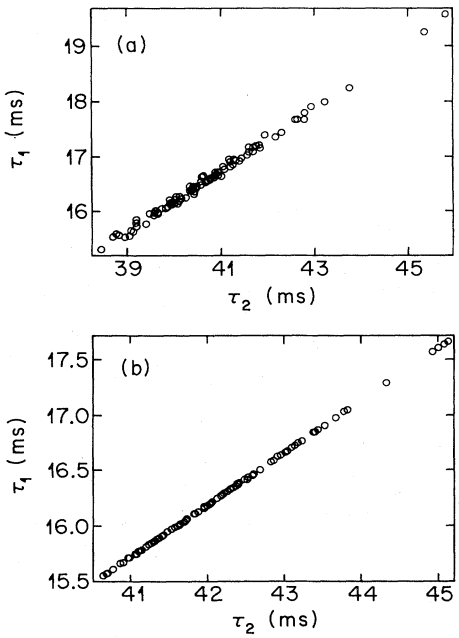

FIG. 6. Time lengths τ_1 and τ_2 of the quiescent phases before the first and second pulse after Q quenching, for $T_q=2$ ms. Notice the strong correlation between the two for both experiment (a) and EBL simulation (b).

by the noise fluctuations of the field in the NMR coil. Indeed, the line $Y=0$ is invariant for Eq. (22) and a nonzero magnetization Y can be built up only if the system is perturbed. Then, the trajectory in the (Y,Z) plane consists of a number of large loops, having a long "quiescent" part close to the Z axis, which become smaller and smaller until the motion is definitely attracted by the fixed point (Y_1,Z_1). Typical laser transients showing the time evolution of the output voltage $v(t)$ are displayed in Fig. 4 for three different quenching times. Clearly, the longer T_q, the longer the time interval between the first and the second pulse. Indeed, for large T_q, the second pulse is also triggered by noise, since the signal amplitude drops nearly to zero.

The above observations show that a quatitative test of the model can be made only by explicitly taking into account the noise. It is assumed that the major source is due to the thermal noise current in the coil. Its rms contribution $\bar{B}_n$ to the field at the absolute temperature T is given by

$$\bar{B}_n=\sqrt{\mu_0 k_B TQ\Delta\nu/lR^2 2\pi^2\nu_a}\ , \tag{24}$$

where k_B is Boltzmann's constant, $\Delta\nu$ the LC-circuit bandwidth, ν_a its resonance frequency, and R the radius of the wire. Inserting realistic numbers yields $\bar{B}_n\approx 4.7\times 10^{-12}$ T. Hence the transients can be numeri-

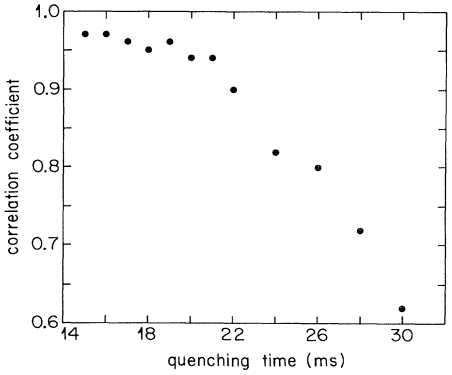

FIG. 7. Correlation coefficient from a linear regression applied to (τ_1,τ_2) plots, as in Fig. 6, obtained for 12 different quenching times T_q. The correlation is lost for $T_q > 20$ ms.

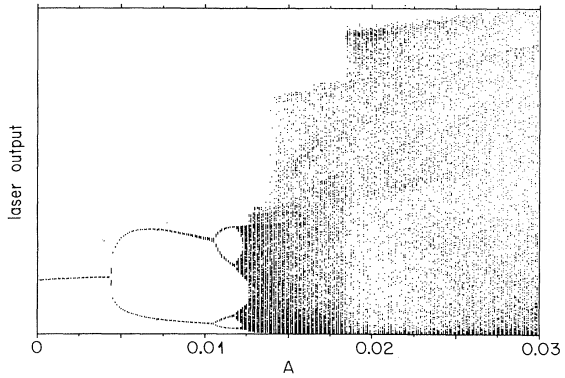

FIG. 8. Bifurcation diagram for the Q-modulated NMR laser obtained by sweeping the forcing amplitude A downwards.

cally generated by turning Eqs. (10) into Langevin equations with two additive Gaussian noise terms with amplitude $\bar{B}_n$. However, since the measured output signal $v(t)$ is proportional to the modulus of the magnetization, it is convenient to integrate Eq. (22), rewritten for the variable $W=\ln Y$, and then to transform back to the physical variable M_v. In this way, we prevent noise from changing the sign of the Y variable in Eq. (22), which should not be allowed. Computed and experimental transient signals are reported in Figs. 5(a) and 5(b), respectively. The numerical simulation has been performed with the CBL (dashed line) and EBL (solid line) models, the latter yielding the best fit with the real data for $\alpha \approx 0.607$ m/A. The quenching time was $T_q = 20$ ms. The agreement with the experiment is evident for the EBL model, whereas the CBL model grossly fails to reproduce both amplitude's decay and oscillation frequency (given by $\gamma_{\rm rel}$ and $\nu_{\rm rel}$, respectively). These results illustrate the enormous effect of the small correction term $\alpha M_v/3 \approx 3\times 10^{-3}$ on the dynamics.

Finally, the noise amplitude $\bar{B}_n$ could be independently estimated by fitting the laser output with EBL simulations. We recorded a sequence of 100 independent transients, all starting after a quenching time $T_q = 2$ ms from the initial state $\mathbf{M}_t^s$, and measured the times τ_1 and τ_2 at which the first two pulses occurred. As it is clearly seen in Fig. 6, they are strongly correlated. The numerical simulation from the EBL model (b) confirms the excellent agreement between experiment and theory. The measurement was then repeated for various quenching times T_q. The corresponding correlation coefficient for the scattered data points (τ_1,τ_2) is plotted versus the quenching time in Fig. 7. An evident loss of correlation occurs for $T_q > T_q^c \approx 20$ ms. Beyond this value, noise disrupts the deterministic dynamics. An estimate of $\bar{B}_n$, obtained by fitting the data in Fig. 7 with those obtained from the EBL model, yielded $\bar{B}_n = 1.2\times 10^{-12}$ T (at the temperature of 4.2 K).

B. Conventional analysis of chaotic motion

A common visualization of the transition to chaos consists of a bifurcation diagram, where a few values $v(t)$ of a coordinate, measured at equally spaced times $t = k\Delta t$, are reported as a function of the control parameter, after transients have died out (Collet and Eckmann, 1980; Cvitanović, 1984). The plot in Fig. 8 has been obtained by sweeping the amplitude A at a fixed frequency ω. A period-doubling cascade is clearly visible, with the first bifurcations occurring at $A \approx 0.0047$ (period $1 \rightarrow 2$),

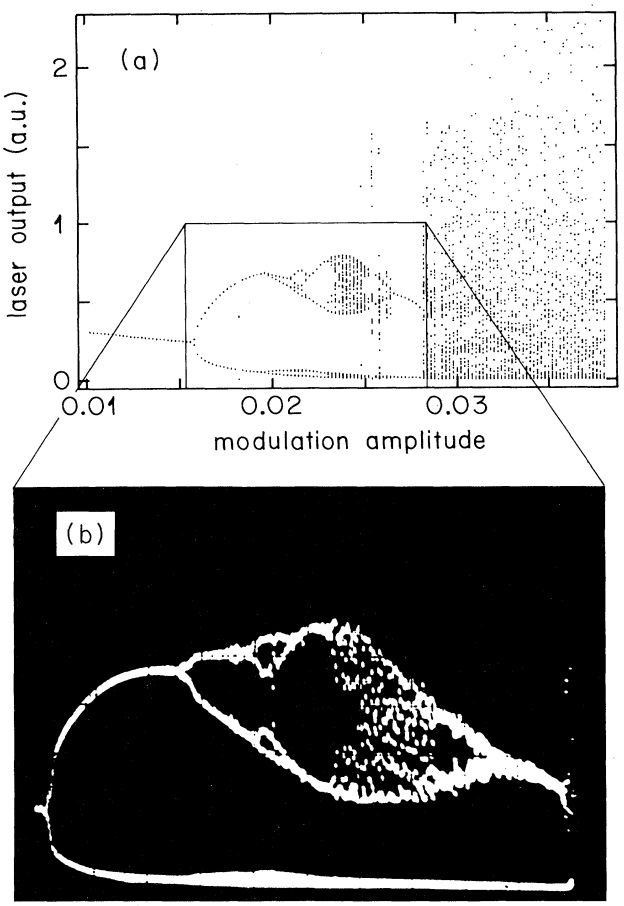

FIG. 9. Bifurcation diagrams, as in Fig. 8, but with a different forcing frequency. The diagram from the EBL model (a) is compared with an early experimental one (b) observed on the oscilloscope screen.

$A \approx 0.0105$ (period $2 \rightarrow 4$), and $A \approx 0.0117$ (period $4 \rightarrow 8$). The abrupt expansions of the region visited by the trajectory (at $A \approx 0.014$ and $A \approx 0.018$) are crises; they will be studied in detail later. Very similar diagrams have been obtained from the EBL model. In Fig. 9 an early experimental observation on the oscilloscope screen (b) can be compared with the corresponding simulation (a). The agreement between experiment and EBL model is once more confirmed. However, the CBL model yields very similar plots.

A more significant test is provided by the comparison between phase diagrams, i.e., graphical representations of the types of motion (either stable periodic or chaotic) exhibited by the system in an extended portion of the (ω, A) plane. In Fig. 10, we report experimental (a) and EBL (b) diagrams, where the main islands of stable periodic behavior are indicated together with the large chaotic region. Multistability occurs quite often. Most of the structure in the two pictures coincides, although some discrepancy exists (probably caused by uncertainty about the value of the other model parameters a, c, or β).

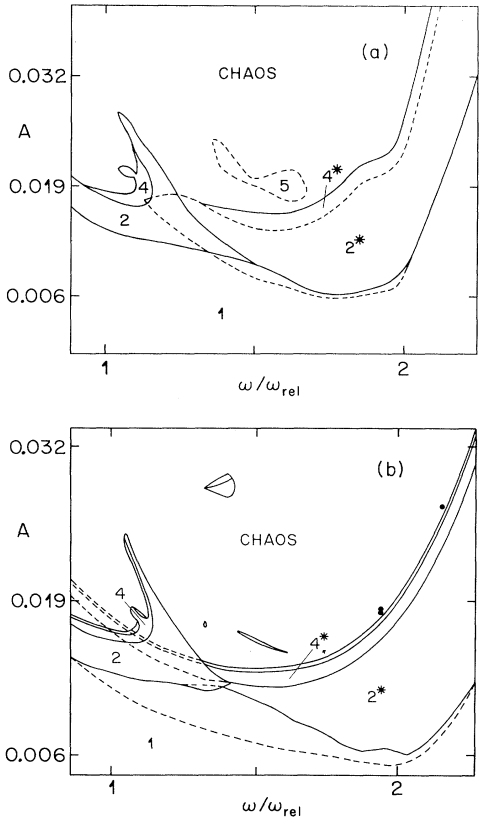

FIG. 10. Phase diagrams for the Q-modulated NMR laser. Experiment (a) and EBL model (b) are in good agreement, considering the uncertainty in the physical constants. The main regions with stable periodic motion are indicated. The periods 2 and 4 labeled by an asterisk are distinct from the unlabeled ones. Notice the coexistence of different types of motion in a few regions. The solid circles in (b) indicate the parameter values for which the periodic-orbit analysis has been carried out.

The conventional analysis of chaotic motion proceeds with estimates of dimension, entropy, and Lyapunov exponents of typical attractors of the system (Grassberger *et al.*, 1991). We briefly review these concepts with the purpose of illustrating further the phenomenology of the laser. It will also be clear that such global indicators do not represent a tool for a univocal identification of an appropriate model.

The estimates have been carried out with both experimental and simulated time series. In the former case, the signal $v(t)$ is sampled at a frequency ν_s to yield a sequence of $N \approx 8 \times 10^5$ data points measured with a 12-bit resolution. Usually, ν_s is taken about 4 times larger than the forcing frequency $\omega/2\pi$ and incommensurate with it for estimates of fractal dimensions. The delay time is accordingly $\tau = 1$. A different choice is needed for the extraction of periodic orbits. The embedding dimension E is varied between 3 and 20 or more.

Generalized dimensions (Renyi, 1970; Mandelbrot, 1982) and entropies (Grassberger and Procaccia, 1984; Eckmann and Procaccia, 1986) have been computed with the nearest-neighbor method (Badii and Politi, 1984a, 1984b; Broggi, 1988). A subset $\{\mathbf{y}_j\}$ of $r = 10^3$ reference points is chosen at random from the time series with respect to the Lebesgue measure. Since the data points are sampled uniformly in time, this procedure is equivalent to selecting points at random on the attractor according to the natural invariant measure m (Eckmann and Ruelle, 1985). For each point $\mathbf{y}_j$, one orders its nearest neighbors from the first to the kth as they are found in a set of n other points of the attractor (also chosen at random with respect to m). The distance $\delta_{j,k,E}(n)$ from $\mathbf{y}_j$ to the kth neighbor clearly cannot increase with the number of points n. Noticing that k/n is an approximation of the probability of finding a point in a ball centered at $\mathbf{y}_j$ having size $\delta_{j,k,E}(n)$, one may define a local dimension α_j in terms of the mass-volume relation (Grassberger *et al.*, 1988)

$$\frac{k}{n} \sim \delta_{j,k,E}(n)^{\alpha_j} , \tag{25}$$

where the symbol $\sim$ indicates the leading behavior in the limit $n \rightarrow \infty$ [which corresponds to $\delta_{j,k,E}(n) \rightarrow 0$]. An average dimension, the dimension function $\tilde{D}(\gamma)$ (Badii and Politi, 1984b), is then computed as

$$\frac{1}{\gamma} \ln \frac{1}{r} \sum_{j=1}^{r} \delta_{j,k,E}^{\gamma}(n) \sim \frac{-1}{\tilde{D}(\gamma)} \ln(n/k) , \tag{26}$$

for various values of γ. The implicit relation between $\tilde{D}(\gamma)$ and the Renyi dimensions D_q (Renyi, 1970) is

$$\tilde{D}(\gamma) = D_q , \quad \text{for } \gamma = (1-q)D_q . \tag{27}$$

For the special case $\gamma = 0$, one obtains the information dimension D_1. Indicating with $\langle f \rangle$ the average of an observable f computed as in Eq. (26) by summing over r domains, one obtains the generalized metric entropies $\tilde{K}(\gamma)$ through the relations

$$\ln\langle \delta_{k,E}^{\gamma}(n)\rangle \sim \frac{\gamma}{\tilde{D}(\gamma)}[\tau E\tilde{K}(\gamma)-\ln n] \quad \text{if } \gamma\neq 0 , \tag{28}$$

and

$$\langle \ln\delta_{k,E}(n)\rangle \sim \frac{1}{\tilde{D}(0)}[\tau E\tilde{K}(0)-\ln n] \quad \text{if } \gamma=0 , \tag{29}$$

in the large-n limit. Although the precision can be improved when a large number of points is available, such asymptotic estimates are disturbed by the presence of lower-order corrections (e.g., $\ln\ln n$) to the leading behavior. The nonhyperbolicity, moreover, determines a large spread in the values of the local dimensions α_j (and in analogously defined local entropies). Since the probability $p\approx k/n$ is the same for each ball, this method is called fixed mass. The dual approach consists of covering the attractor with balls of constant radius ε and estimating the probability $P(\varepsilon)$ of each of them. Accordingly, one obtains the usual definition of generalized Renyi dimension (Renyi, 1970)

$$\langle P^{q-1}(\varepsilon)\rangle \sim \varepsilon^{(q-1)D_q} \tag{30}$$

in the limit $\varepsilon\to 0$. The presence of balls with a very small population renders this approach impractical for $q<1$ (Grassberger and Procaccia, 1983,1984; Grassberger *et al.*, 1991).

By testing the scaling behavior of the probability $P(\varepsilon,n)$ of finding a trajectory of length n within a distance ε from a reference orbit, one can estimate the generalized metric entropy K_q as

$$\langle P^{q-1}(\varepsilon,n)\rangle \sim e^{-n(q-1)K_q} \tag{31}$$

for $n\to\infty$ and sufficiently small ε. For $q=1$, one recovers the usual Kolmogorov-Sinai entropy. The relation between K_q and $\tilde{K}(\gamma)$, defined above, is analogous to Eq. (27). The fixed-mass method is better suited for estimates corresponding to $q\geq 1$ and for higher dimensions than the fixed-size method (Kostelich and Swinney, 1987; Broggi, 1988).

In all cases, deviation either from a pure power-law dependence on ε or δ for dimensions or from a pure exponential dependence on n for entropies affects the averages in such a way that convergence to the asymptotic behavior may be very slow. This is the rule in nonhyperbolic systems and is particularly evident at certain "critical" values of q or γ. This phenomenon has been interpreted in terms of phase transitions using the thermodynamic formalism for dynamical systems (Halsey *et al.*, 1986; Grassberger *et al.*, 1988; Badii, 1989a; Beck and Schlögl, 1993).

Improved convergence can be obtained by labeling each individual subdomain (or orbit) with the help of symbolic dynamics. In this way, the asymptotic scaling can be tested for each symbolic sequence separately before performing the averages. This technique is related to the transfer-matrix method of statistical mechanics (Feigenbaum *et al.*, 1986; Feigenbaum, 1988; Mayer, 1991; Badii, 1993; Beck and Schlögl, 1993). Since a discussion of this topic exceeds the purpose of the present work, we refer the reader to the relevant literature.

In Fig. 11, we show a two-dimensional projection of a strange attractor of the NMR laser with the log-log plot of Eq. (26) which yields the information dimension D_1 from the slopes of the curves $\langle \ln\delta_{k,E}(n)\rangle$ vs $\ln n$ in the asymptotic region (in the figure, an arbitrary base has been used for the logarithm). The slopes usually exhibit convergence for $E>2D+1$, extending over several values of E. In this region, if the number of data points is large enough, the dimensions $\tilde{D}_k(\gamma)$ corresponding to different nearest-neighbor orders k agree. The value given by the highest k is usually taken as the estimate of the fractal dimension. The information dimension D_1

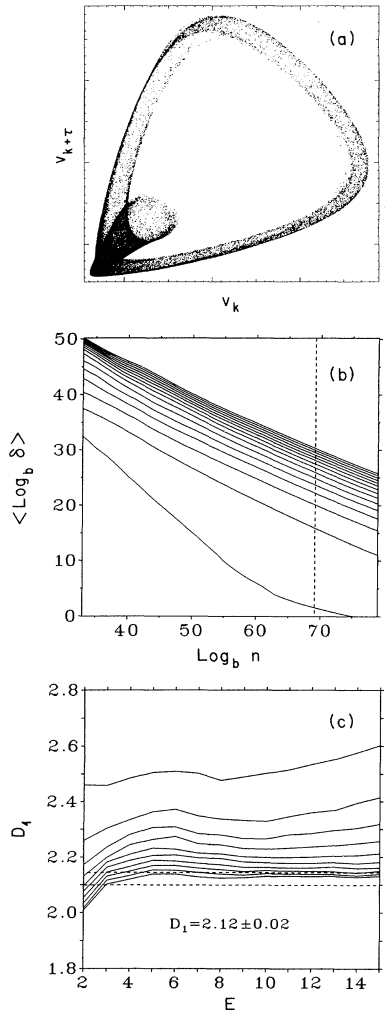

FIG. 11. (a) Two-dimensional projection of a strange attractor in the Q-modulated case. (b) Dependence of the logarithmic average of the nearest-neighbor distance δ on the number n of data points, shown for embedding dimension E between 1 and 15. Notice the smoothness and the parallelism of the curves, especially in the asymptotic region (to the right of the dashed line). (c) Estimated information dimension D_1 as a function of the embedding dimension, for different nearest-neighbor order $k=2,4,\ldots,20$.

lies in the range [2.1,2.5] for all chaotic attractors in the (ω, A) plane shown in Fig. 10 (Ravani *et al.*, (1988). Hence the minimum embedding dimension that ensures a smooth reconstruction of the original phase-space dynamics is $E_{\min}=2D_1+1\approx 5-6$ (Sauer *et al.*, 1991). The metric entropy K_1 lies in the range [0,0.45] in units of $1/T_0$, where T_0 is the period of the forcing term. Finally, the "standard" analysis was completed by the evaluation of the Lyapunov exponents. We used an algorithm adapted from those proposed in Eckmann *et al.* (1986) for experimental data and in Benettin *et al.* (1980) for differential equations. With increasing embedding dimension, the positive exponent λ_1 approaches values in good agreement with K_1 (recall that K_1 is upper-bounded by the sum of positive Lyapunov exponents). These results have been confirmed using an indirect evaluation of the positive and the negative Lyapunov exponents of the system, based on a dimension measurement performed on a low-pass filtered output signal (Badii *et al.*, 1988). In Fig. 12, we show a bifurcation diagram (a) of the Q-modulated laser, obtained at $\omega\approx 1.8\omega_{\rm rel}$, and the Lyapunov exponents (b) in a four-dimensional embedding, plotted as a function of the modulation amplitude A.

Although the experimental results appear to be in better agreement with the EBL model than with the conventional one, the relatively low precision of these estimated characteristics does not permit us to discriminate clearly between the two. Even taking into account the spectra of the local dimensions and entropies [the latter being defined as $\kappa=-\ln P(\varepsilon,n)/n$ in a small neighborhood of size ε around a reference orbit of length n], we cannot distinguish them unequivocally.

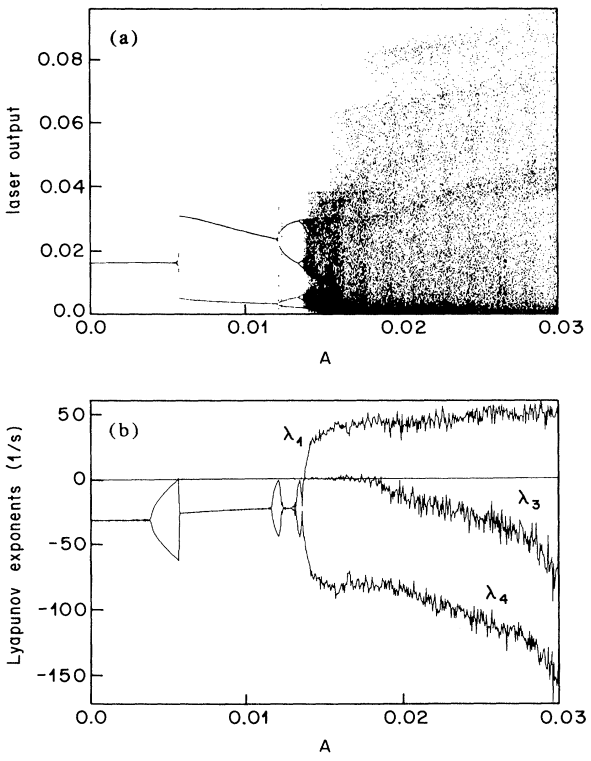

FIG. 12. Upward-sweep bifurcation diagram for the Q-modulated case (a) and corresponding average Lyapunov exponents (b) from the EBL model. The second Lyapunov exponent λ_2 (not indicated) is identically zero.

C. Periodic orbits

The simple analysis illustrated above, although quantitative, is not sharp enough to assess the suitability of the EBL equations for a description of the NMR laser dynamics. A much more stringent verification is represented by the comparison of the periodic orbit structure of the real and simulated systems. Not only must the number and length of the periodic orbits agree, but also their shape and the probability with which the aperiodic trajectory of the chaotic system visits their neighborhoods.

Time series consisting of $N=8\times 10^5$ points were

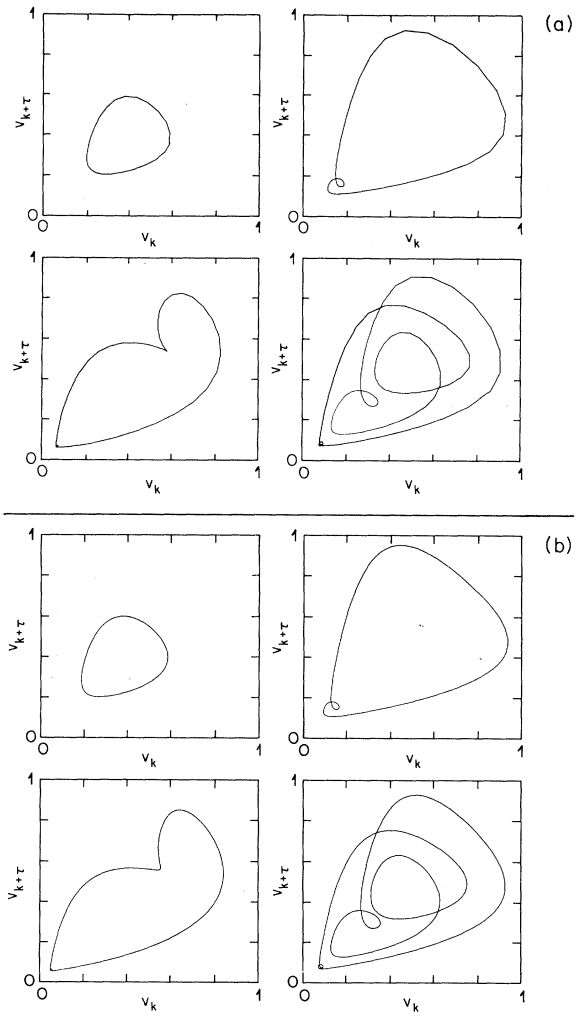

FIG. 13. Two-dimensional projections of four unstable periodic orbits (periods 1, 2, 3, and 5) extracted from the experimental data (a) and from the EBL model (b).

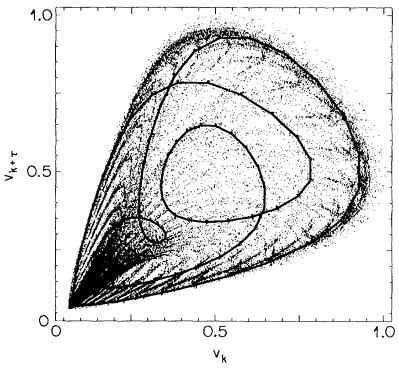

FIG. 14. Projection of the period-5 orbit of Fig. 13, superimposed on the strange attractor.

recorded with a sampling frequency $\nu_s = 25/T_0$, where $T_0 = 2\pi/\omega$ is the period of the forcing term: we collected $n_p = 25$ points per period. The delay time for the embedding was $\tau = 5$. Hence the embedding window $E\tau$ covered one period for an embedding dimension $E = 5$. All unstable periodic orbits up to order 9 (i.e., of period $9T_0$) were located. A Newton method was used to detect the periodic orbits of the EBL model. All cycles up to order 9 were compared with the experimental ones and found to agree very well for all E between 6 and 16. Some experimental and numerical periodic orbits are shown in Fig. 13. In Fig. 14, we show a period-5 orbit superimposed on the corresponding strange attractor.

As a preliminary step towards a hierarchical

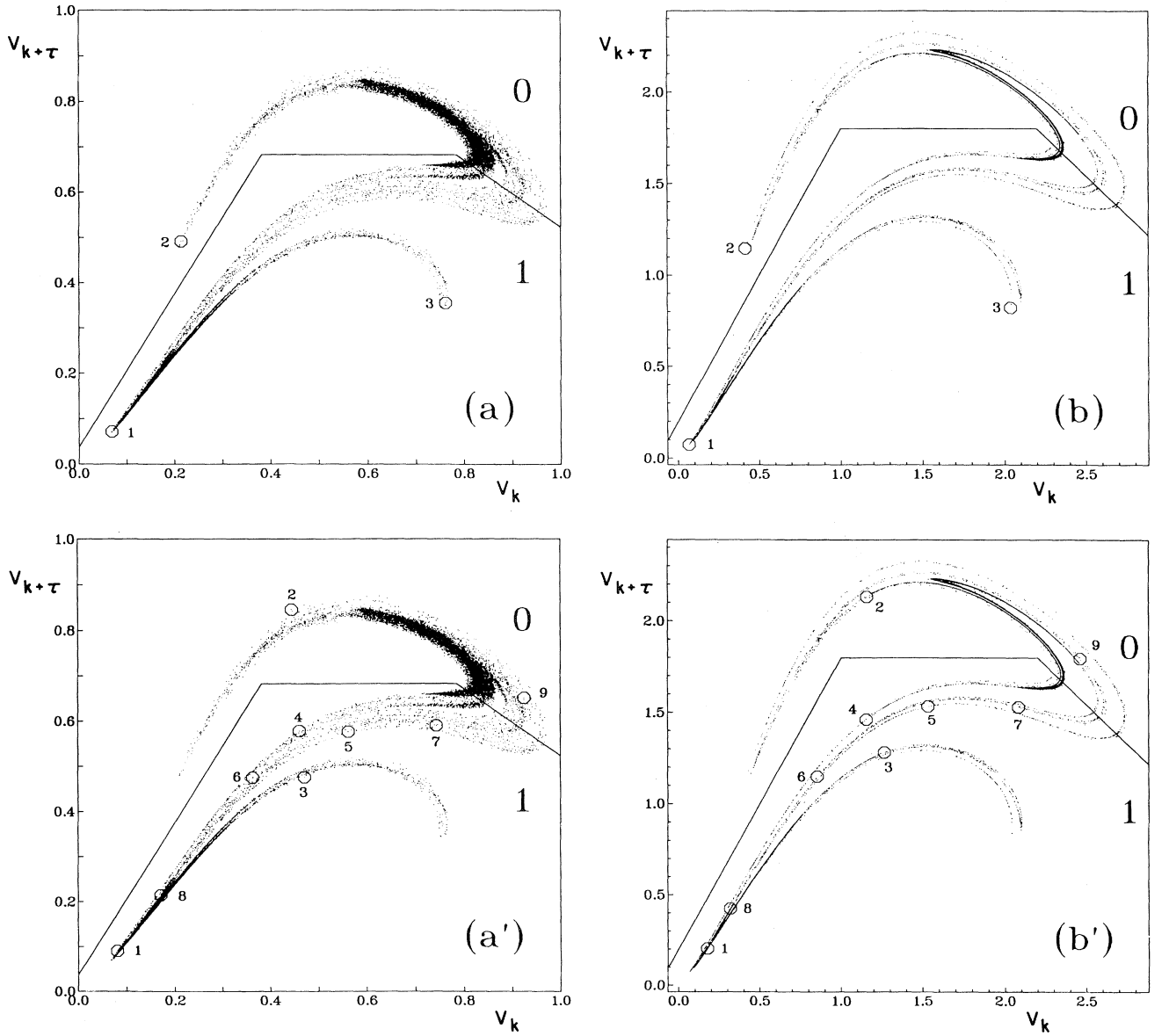

FIG. 15. Two-dimensional projections of the Poincaré section for $A = 0.018$ and $\omega = 0.03168$. The intersection points of the period-3 (a,b) and of a period-9 (a',b') cycle are labeled in order of their occurrence: (a,a') experiment, (b,b') EBL model. The solid line represents the binary partition with elements labeled 0 and 1.

classification of the dynamics of the NMR laser, we constructed Poincaré sections Σ in each embedding space by considering points $\mathbf{x}_i$ which lie n_p time units apart from one another. Two-dimensional projections of the strange attractor in Σ are shown in Fig. 15. The embedded coordinates from the experimental (a,a') and numerical (b,b') time series are shown for $A=0.018$ and $\omega=0.03168$. The intersection points of a period-3 orbit (a,b) and of a period-9 orbit (a',b') with Σ are indicated by open circles. Notice the striking similarity between the two data sets. The CBL model is unable to reproduce these orbits with good precision.

A symbolic dynamical encoding of the attractors was achieved through a binary partition (Finardi, 1993) $\mathcal{B}=\{B_0,B_1\}$ which distinguishes all periodic points up to order 9. The curve defining $\mathcal{B}$ is also displayed in Fig. 15. Three orbits in a three-dimensional representation are shown in Fig. 16 with their labels (Tufillaro, Holzner, Flepp, Finardi, and Badii, 1991).

The language $\mathcal{L}$ for these parameter values can be described by a full binary tree over the two primitive words $w_1=1$, $w_2=01$ (Badii, 1990), for both experiment and model, up to hierarchical level 4 (the longest orbit of which is 01010101). In fact, the only experimental forbidden sequence is 00, whereas in the numerical simulation also three strings of length 9 are not allowed. Therefore, at the experimental resolution, the symbolic dynamics can be represented by the 2×2 matrix

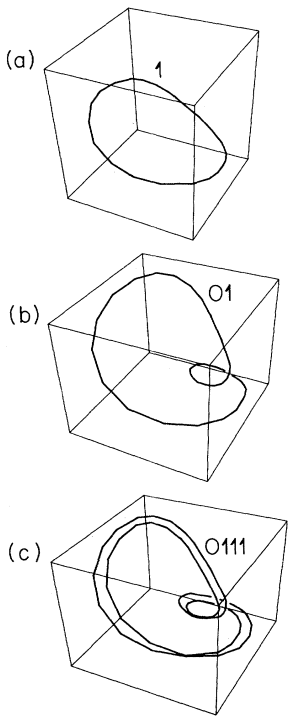

FIG. 16. Three-dimensional representation of three low-order orbits, together with their symbolic label.

$$\mathbf{A}=\begin{bmatrix}0 & 1\\ 1 & 1\end{bmatrix} \tag{32}$$

with entries $A_{ij}=1$ if the transition $i\rightarrow j$ is allowed and $A_{ij}=0$ otherwise. The row and column indices i and j run over the symbols 0 and 1: the zero entry indicates that $S=00$ is forbidden. The topological entropy K_0 of this language is just the logarithm of the largest eigenvalue μ_1 of $\mathbf{A}$: i.e., $K_0=\ln[(1+\sqrt{5})/2]=\ln\mu_1$. Since other prohibitions exist for longer orbits, this estimate is only an upper bound.

The prime cycles (i.e., those which cannot be written as periodic repeats of shorter ones; see Cvitanović, 1988) have the following form: w_1, w_2, w_2w_1, $w_2w_1^2$, $w_2^2w_1$, $w_2w_1^3$, $w_2^2w_1^2$, $w_2w_1^4$, $w_2^2w_1^3$, $w_2w_1^5$, $w_2^3w_1^2$, $w_2^2w_1^4$, $w_2w_1^6$, $w_2^2w_1^5$, $w_2w_1^7$, where w^n denotes the nth repetition ("power") of word w. The tree that allocates all words in the language $\mathcal{L}$ constitutes an invariant topological characterization of the system. The nearly full coincidence found between measured and numerical data (confirmed for the other time series, which will be discussed in the next section) clearly shows that the EBL model indeed describes the experimental observation up to the available resolution. A further test of the reliability of the partition is made by comparing the metric entropy K_1 evaluated with the fixed-mass method and according to its definition in terms of symbolic sequences: the latter obtained by estimating the probability $P(S)$ of observing an n-symbol sequence $S=s_1s_2\cdots s_n$ in the symbolic signal induced by $\mathcal{B}$ and by computing

$$K_1=\lim_{n\rightarrow\infty}-\frac{1}{n}\sum_{S:|S|=n}P(S)\ln P(S)\ , \tag{33}$$

where the sum runs over all sequences S with length $|S|=n$. The agreement between this value and the one obtained from Eq. (29) shows that the partition is generating within the experimental and statistical errors.

D. Crisis

The symbolic approach provides a hierarchical description of the dynamics, which has been employed above for a topological comparison between experiment and model. This analysis can be extended to include the metric features of the Poincaré map $\mathbf{F}$. A clear illustration of the utility of symbolic dynamics in this new context appears in the study of what are called crises (Grebogi, Ott, Romeiras, and Yorke, 1987). These are sudden changes occurring in strange attractors when a control parameter reaches some critical value A_c. The NMR laser shows several phenomena of this type when the amplitude A is slowly increased, in a wide range of frequency values.

Three different types of crisis have been so far identified (Grebogi, Ott, Romeiras, and Yorke, 1987). In the first two classes, the chaotic attractor either disappears or widens, respectively. In the third one, different

strange sets merge. These transitions are associated with a characteristic temporal scaling of trajectories above the critical point. We mostly investigated the second case, in which the orbit intermittently bursts out of the phase-space region within which it was confined before the crisis (core attractor). The average time τ between the bursts of this so-called crisis-induced intermittency obeys the power law $\tau(A) \propto |A - A_c|^{-\gamma}$ in the vicinity of the critical value A_c. The scaling exponent γ has been predicted to lie in the interval $[\frac{1}{2}, \frac{3}{2}]$ (where the extrema correspond to the strongly dissipative and conservative limits, respectively; Grebogi, Ott, Romeiras, and Yorke, 1987).

At $A = A_c$, the attractor (the closure of the unstable manifold of some periodic orbit γ_1) collides with the stable manifold of an unstable periodic orbit γ_2. If γ_1 and γ_2 are just the same orbit, the crisis is called homoclinic; otherwise, it is called heteroclinic. The exponent γ for the heteroclinic crisis is given by $\gamma = \frac{1}{2} + \lambda_1/|\lambda_2|$, where λ_1 and λ_2 are the expanding and contracting Lyapunov exponents of the orbit γ_1, respectively (Grebogi, Ott, Romeiras, and Yorke, 1987).

The first experimental evidence of a crisis-induced intermittency via a heteroclinic tangency was obtained in the Q-modulated NMR laser (Finardi *et al.*, 1992) with modulation frequency $\nu_m = 120$ Hz, corresponding to about twice the intrinsic relaxation frequency. The modulation amplitude A was varied in the range [0.0180,0.0187], where the former value lies slightly below the crisis point $A_c \approx 0.01802$ and the latter well above it. The time series were recorded at 14 different A values by sampling the laser output with a frequency $\nu_s = 24\nu_m$. They consisted of $N = 10^5$ 12-bit integers. The value of the scaling exponent γ could be estimated with high accuracy by constructing the symbolic dynamics of the system. The results have been confirmed through independent calculation of the Lyapunov exponents both for the experimental data and for the EBL model.

Once an approximate generating partition is obtained as explained above, the mechanism of the crisis is readily reformulated for the associated shift map $\hat{\sigma}$. In fact, below the crisis, all points belonging to the subset B_0 are mapped to B_1 in one iteration; the string 00 is forbidden. At the crisis, the chaotic trajectory starts visiting a close neighborhood of the new unstable periodic orbit γ_2, which, in our experiment, is a period 3 with label $w_3 = 001$. Hence, after the onset of the crisis, the string 00 is no longer forbidden. The new, wider attractor is associated with the collision with the orbit γ_2. Recall that the "old" period-3 orbit γ_1 is labeled by $w_2 w_1 = 011$. In Fig. 17, we report a two-dimensional projection of the strange attractor of **F** below the crisis (a and b, corresponding to experiment and EBL model, respectively), with the points of γ_1, and after the crisis (a' and b', with the same convention), with the points of γ_2.

The symbolic signal after the crisis consists of combinations of the three primitive words w_1, w_2, and w_3. The determination of a generating partition allows detecting very precisely when the trajectory enters the "new" region in phase space. In fact, if sequence 00 occurs, the second 0 is part of the new branch. All points contained in the partition element B_{00} are mapped outside the core attractor. They can be reached only from a small neighborhood of the point marked by a 1 in Fig. 17 (a', b'). Notice the smallness of the distance (in two-dimensional projection) between the two period-3 points (1 and 2) on the opposite sides of the partition line and between the first points (1 and 1) of the two different period-3 orbits. No comparable accuracy can be obtained by simply setting a (necessarily arbitrary) threshold in a time plot $x(t)$ vs t of some system observable x (which corresponds to embedding the data in just one dimension).

With our criterion, we have estimated the average time τ spent in the core and determined the critical exponent γ from the slopes of the curves $\log\tau(A)$ vs $\log|A - A_c|$, displayed in Fig. 18. The values obtained from experiment and model are $\gamma_{\rm exp} = 1.02 \pm 0.05$ and $\gamma_{\rm mod} = 1.10 \pm 0.05$, respectively. We finally computed γ in terms of the Lyapunov exponents of the orbit γ_1, evaluated from the eigenvalues of a linearized map around a point of γ_1 in the Poincaré section Σ. We obtained $\gamma_{lya} = 1.0 \pm 0.1$

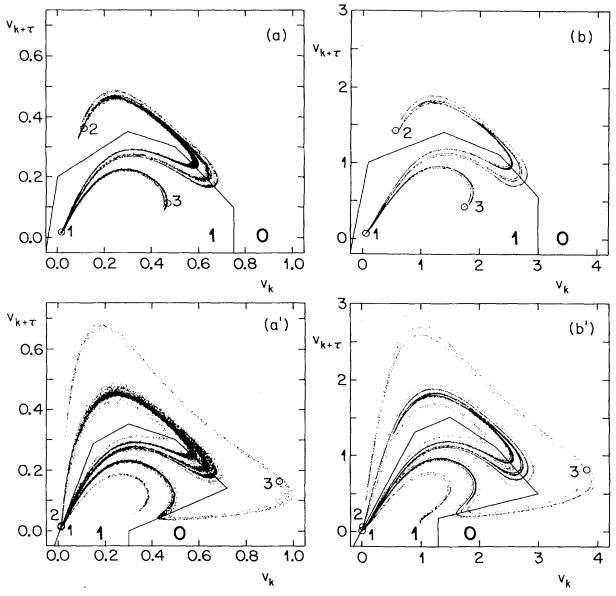

FIG. 17. Poincaré sections obtained from the experimental data at $A = 0.0180$ (a, b), below the crisis, and at $A = 0.0185$ (a', b'), above the crisis, for $\omega = 0.03168$. The intersection points (open circles) of the old, unstable period-3 orbit $\gamma_1(a, b)$ and of the new one, $\gamma_2(a', b')$, are numbered in order of occurrence in time (their symbolic sequences being 011 and 001, respectively). The solid curves indicate an approximation to a generating partition with elements 0 and 1. The first two intersection points 1 and 2 in (a', b') lie on opposite sides of the partition. The primed figures correspond to the EBL model.

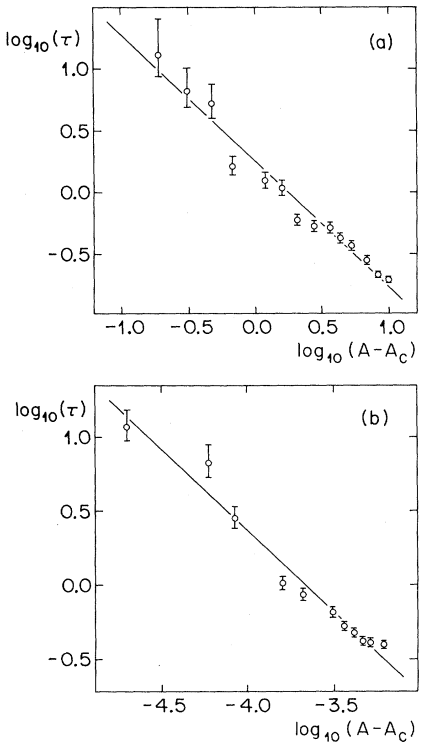

FIG. 18. Average time $\tau(A)$ between successive bursts as a function of $|A-A_c|$, obtained from experiment (a) and EBL model (b). The critical exponents $\gamma_{\rm exp}=1.02\pm0.05$ (a) and $\gamma_{\rm mod}=1.10\pm0.05$ (b) are determined from the slopes of the straight lines obtained by a least-squares fit in a doubly logarithmic scale.

(Kantz *et al.*, 1993), in agreement with the direct estimates.

V. CONTROL OF THE CHAOTIC FLOW

The method for the identification of the unstable periodic orbits has been adapted to a real-time process for possible control of the chaotic NMR laser. In this section we report results obtained with the control procedure proposed in Ott *et al.* (1990a, 1990b), applied to the stabilization of low-order orbits in the Q-modulated case. We illustrate the improvement obtained with a new control method that solves some difficulties arising with the original one (Reyl *et al.*, 1993). The motion in the chaotic regime is thereby constrained to a close neighborhood of some unstable periodic orbit. This result is usually carried out by applying small, carefully chosen perturbations to a control parameter. The method proposed in Ott *et al.* (1990a) requires that, after the displacement, the trajectory lie as close as possible to the stable manifold of the target orbit γ, which is previously located as discussed in Sec. III. The flow around γ is approximated by means of a matrix $\mathbf{M}$, estimated through a least-squares fit. A number m of embedded data points is first found in an ε ball $B_\varepsilon(\mathbf{x}_0)$ around a reference point $\mathbf{x}_0$ on γ. For stability reasons, we required that these points remain close to γ for a whole embedding window $E\tau$ both in the past and in the future. As usual, it is assumed that the target orbit is of the saddle type, so that its invariant manifolds can be identified with the eigendirections of the matrix $\mathbf{M}$. Finally, the sensitivity of the motion on the control parameter p is evaluated by comparing $\gamma(p=0)$ with the perturbed orbit $\gamma(p)$, which is also to be extracted from the observed data. For the case in which only one unstable direction exists, the required correction is given by (Ott *et al.*, 1990a)

$$p=\lambda_u(\lambda_u-1)^{-1}[(\xi-\xi_0)\cdot\mathbf{f}_u]/(\mathbf{g}\cdot\mathbf{f}_u)\ , \tag{34}$$

where the curve γ has been cut by a Poincaré section Σ through $\mathbf{x}_0$, yielding the point ξ_0. The value p hence depends on the current position ξ on Σ, on the unstable eigenvalue λ_u of $\mathbf{M}$, and on the projection of the difference vector $\xi-\xi_0$ along the contravariant basis vector $\mathbf{f}_u$. The overall magnitude is finally weighted by the term $\mathbf{g}\cdot\mathbf{f}_u$, where $\mathbf{g}=\partial\xi_0(p)/\partial p|_{p=0}$ represents the dependence of the system on the perturbation.

This method keeps the dynamics around the target orbit at the expense of very little energy input; moreover, it can be applied, in principle, to higher-dimensional systems (Ott *et al.*, 1990b). However, difficulties arise when noise is non-negligible (Ditto *et al.*, 1990) or when several unstable or complex eigenvalues occur, which require a different equation than (34). To overcome the latter problem, a modified technique was recently proposed (Auerbach *et al.*, 1992) which considers perturbations of scalar quantities. No application to real experiments has yet been carried out.

In the case of the NMR laser, with embedding dimension 4 to 6, the major source of inaccuracy comes from the evaluation of the eigenvalues with the corresponding contravariant vectors and of the "flow derivative" $\mathbf{g}$: in fact, they fluctuate considerably from run to run, so that the control is not frequently reproducible in certain regions of parameter space. Therefore we have implemented an algorithm that still retains the positive features of the original method, without, however, being affected either by the occurrence of more than one unstable direction or by the possible complexity of the eigenvalues. The control condition that replaces Eq. (34) is obtained by requiring that the expected deviation of the orbit from the target be minimized by our choice of p (minimal expected deviation method or MED). Our prediction is based on the same matrix $\mathbf{M}$ as in Eq. (34), although the dynamics may now be approximated by a more general nonlinear map as well. No estimate of the eigenvalues and of the corresponding contravariant vectors is needed, thus yielding higher reproducibility of the control. The vector $\mathbf{g}$ is, however, still determined as before. An improved estimate might be obtained by recomputing it at each visit of the control ball $B_\varepsilon(\mathbf{x}_0)$ and by averaging in time. Finally, the new method may easily be implemented with several control stations along the target orbit.

We applied both the original and the MED methods to the NMR laser operating with a modulation frequency $\nu_m \in (100,120)$ Hz. Although the operating frequency was about 120 times higher than that of previous experiments (Ditto *et al.*, 1989, 1990; Sommerer *et al.*, 1991a, 1991b), control was achieved under several conditions for the lowest-order periodic orbits. Another important difference is the higher embedding dimension used in the present work and the high precision required for a close return to be accepted. Time series of length $N=1.5\times10^5$ have been analyzed, and the unstable periodic orbits up to order 6 have been located during the acquisition of data points. The dynamics around an interactively chosen unstable orbit γ has been approximated by means of one or more linear maps.

Indicating again with ξ_0 the control point on the Poincaré surface through γ, we can approximate the dynamics from a neighborhood $B_\varepsilon(\xi_0)$ of ξ_0 to itself by

$$\xi_{n+1}-\xi_0 \simeq \mathbf{M}[\xi_n-\xi_0] , \tag{35}$$

where $\mathbf{M}=\mathbf{D}_\xi \mathbf{F}(\xi_0)$ is the Jacobian matrix of the (reduced) Poincaré map $\mathbf{F}$: $B_\varepsilon(\xi_0)\to B_\varepsilon(\xi_0)$. The matrix $\mathbf{M}$ has been estimated with a least-squares procedure that makes use of singular-value decomposition, using a collection of m ($m=50$–100) vector pairs $(\delta\xi,\delta\xi')$ in $B_\varepsilon(\xi_0)$, where $\delta\xi=\xi-\xi_0$ and $\delta\xi'=\mathbf{F}(\delta\xi)$.

A simple noise-reduction method can be implemented to enhance the quality of the fit by discarding the vector pairs for which a considerable discrepancy is found between actual and predicted images of the starting point. A new matrix $\mathbf{M}$ is then estimated from the "cleaned" set of points. The same procedure can be adopted with minor modifications to handle the case of a number $L>1$ of control stations along the target orbit γ. This has been implemented with $L=2$ to 4, obtaining considerably better predictions of the dynamics. One then has L matrices $\mathbf{M}_l$: $B_\varepsilon(\mathbf{x}_l)\to B_\varepsilon(\mathbf{x}_{l+1})$, with $l=1,\ldots,L$ and $\mathbf{x}_{L+1}=\mathbf{x}_1$. The stability properties of γ are determined by the eigenvalues of $\mathbf{M}_l$. At variance with the method by Ott *et al.*, we require that the perturbed point $\xi_{n+1}(p)$ come as close as possible to the control station ξ_0, rather than demanding that it fall onto the stable manifold of γ. Taking, for simplicity, $L=1$, we first rewrite Eq. (35) with explicit dependence of ξ_0 on p as

$$\xi_{n+1}-\xi_0(p) \simeq \mathbf{M}[\xi_n-\xi_0(p)] , \tag{36}$$

where $\xi_0(p_n)\simeq\xi_0(0)+\mathbf{g}p_n$ in a linear approximation (this relation being the operational definition of $\mathbf{g}$). Once the trajectory enters the control ball $B_\varepsilon(\xi_0)$, we seek the value p_n that minimizes the norm $\delta_n=\|\hat{\xi}_{n+1}(p_n)-\xi_0(0)\|$, where $\hat{\xi}_{n+1}(p_n)$ is the prediction for ξ_{n+1} obtained from Eq. (36) taken as a strict equality. The condition that

$$\delta_n=\|\underbrace{p_n(\mathbf{g}-\mathbf{M}\mathbf{g})}_{=:\alpha}+\underbrace{\mathbf{M}[\xi_n-\xi_0(0)]}_{=:\beta}\| \tag{37}$$

be minimized over all values of p_n in a range $[-p_*,p_*]$ is equivalent to asking that the next expected return on the Poincaré section, after application of perturbation p_n, lie as close as possible to the control point. No control is attempted if the computed p overshoots these limits. This yields

$$p_n=p_{\min}\equiv-\frac{\boldsymbol{\alpha}\cdot\boldsymbol{\beta}}{\|\boldsymbol{\alpha}\|^2} , \tag{38}$$

and the minimal distance achievable is $\delta_{\min}=\|-(\hat{\boldsymbol{\alpha}}\cdot\boldsymbol{\beta})\hat{\boldsymbol{\alpha}}+\boldsymbol{\beta}\|$, where $\hat{\boldsymbol{\alpha}}\equiv\boldsymbol{\alpha}/\|\boldsymbol{\alpha}\|$. Notice that if ξ_n is already close to the stable manifold of $\xi_0(0)$, its predicted image will be close to the target point; and Eq. (38) will give a small correction p_n, in agreement with Eq. (34).

This procedure allows fitting the Poincaré map with a generic polynomial function, rather than with a simple linear application, thus leading to improved predictions. Moreover, depending on the computing time restrictions, it is possible to complement it with noise-reduction algorithms. The periodic orbits have been located with relative error $d(\mathbf{x}_i,\mathbf{x}_{i+m})/\varepsilon_i\approx10^{-2}$ under various experimental conditions, where ε_i is the position-dependent ball radius used in the search. The control stations have been set interactively anywhere on the target γ (itself chosen out of a number of close-return orbits).

The statistical reliability of the estimated matrix $\mathbf{M}$ sensibly depends on the position of $\mathbf{x}_0$ on γ, on the ball radius ε, and on the number m of fit-points. The typical χ^2 values, rescaled to ε^2, were in the range $(10^{-3},10^{-1})$, except in the most crowded regions of the attractors (where the dynamics is most affected by the noise), which were not selected for control. The corresponding ε values were in the interval (50,300) for $E=6$ (recall that the data are 12-bit integers: i.e., $v_k\in[0,4096]$). The fits were usually carried out with sets of $m=50$–100 nearest neighbors.

In Fig. 19, we show a portion of the time series $v(t)$ (a) and the corresponding controlling signal (b) during the stabilization of the period-1 orbit with the method by Ott

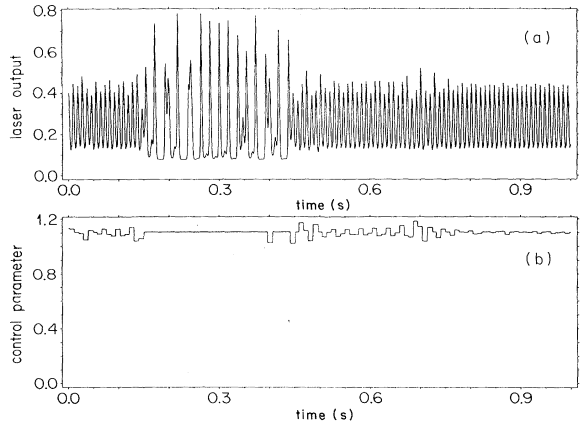

FIG. 19. Time plot of the controlled period-1 orbit (a) and of the controlling signal (b) as produced by the method proposed in Ott *et al.* (1990a, 1990b). The control was switched off at $t=0.15$ s and restarted at $t=0.4$ s.

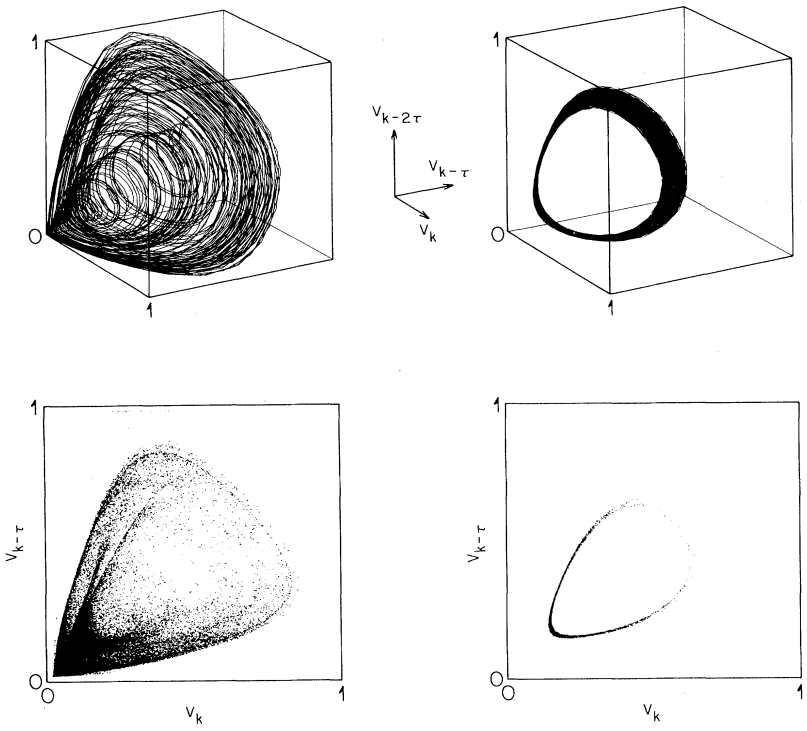

FIG. 20. Two- and three-dimensional representations of the strange attractor without control (left column) and of the period-1 orbit controlled as in Fig. 19 (right column). The parameter values are the same as in Fig. 19.

et al.; in Fig. 20, we report two- and three-dimensional projections of the strange attractor and of the controlled orbit.

The minimal expected deviation technique, being based on the matrix **M** (or on some other predictor) rather than on the eigenvectors $\mathbf{f}_u$, proved to be more efficient than the method by Ott *et al.* for the period-1 cycle. Moreover, the period-2 orbit could also be stabilized in a reproducible way, as well as a period-4 cycle. In both cases, it was sufficient to apply a rather small relative perturbation $A \rightarrow A + p$, with $|p| \leq p_{\max}$ and $p_{\max}/A \leq 0.02$ (see Fig. 21). The recovery time upon external disturbances was also appreciably shorter. No spontaneous outbursts have been observed for times of the order of two hours or more. This technique appears to be less sensitive to noise. The maximal deviation from the target remained below the value $\delta_{\max} \approx 300$ in six dimensions. The output and control signals are displayed in Fig. 21, which refers to the period-2 orbit. The largest eigenvalue of the period-1 orbit is $\lambda_u^{(1)} = -2.0 \pm 0.1$ (in the Poincaré section), whereas that of the period-2 orbit is $\lambda_u^{(2)} = -1.3 \pm 0.1$. The latter orbit, however, passes very close

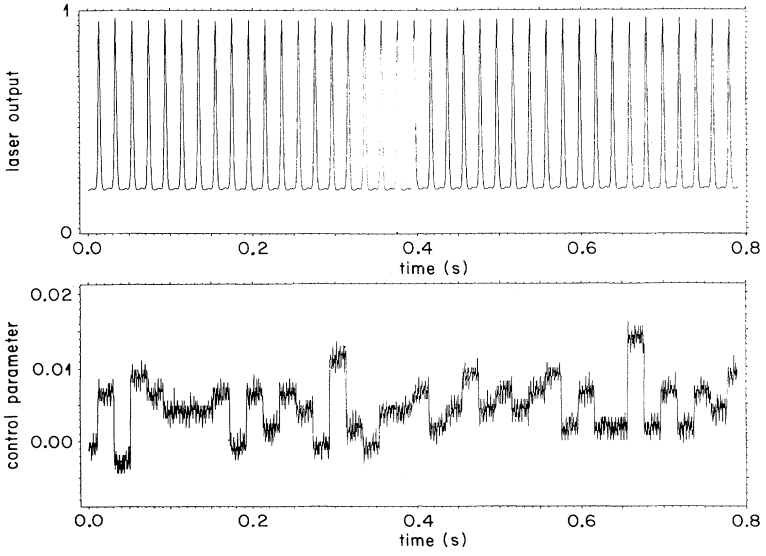

FIG. 21. Unstable period-2 obit stabilized with the minimal expected deviation (MED) method. Upper plot: controlled signal; lower plot: controlling signal. No spontaneous outburst was observed for over two hours of laser activity. Notice the smallness of the controlling-signal amplitude.

to the origin, where the signal-to-noise ratio is small, and is therefore much harder to control.

VI. SUMMARY AND OUTLOOK

The characterization of low-dimensional chaotic systems has gradually moved from the evaluation of simple, global indicators, such as fractal dimensions and entropies (Cvitanović, 1984; Eckmann and Ruelle, 1985; Bergé *et al.*, 1986; Guckenheimer and Holmes, 1986; Schuster, 1988), to distributions of local indicators, synthetized in dimension and entropy spectra (Halsey *et al.*, 1986; Grassberger *et al.*, 1988; Beck and Schlögl, 1993). These quantities can be computed from scalar time series with good accuracy (Mayer-Kress, 1989; Grassberger *et al.*, 1991; Drazin and King, 1992). There are, however, open problems such as the understanding of the symbolic dynamics of nonhyperbolic systems and, in particular, of volume-preserving maps. It is believed that further improvement in this field can be achieved by studying the unstable periodic orbits in the neighborhood of the invariant sets (Auerbach *et al.*, 1987; Cvitanović, 1988; Chaos, 1992).

In the present work, we reviewed recent progress in the analysis of experimental chaotic time series, inspired by this suggestion. In particular, we discussed the requirements that measurements must satisfy in terms of precision and high statistics in order for an accurate analysis to be feasible. The role of noise has also been considered. We illustrated a method for the location of the unstable periodic orbits in embedding space, with special care for reliability tests.

The knowledge of the periodic orbits has been used for the first time to construct approximations to a generating partition in an experimental system. This consists of a nuclear-magnetic-resonance laser which has been chosen for its characteristics of stability and low sensitivity to noise.

The first important result of this analysis was the identification of an extremely accurate differential model for the dynamics, an extension of the conventional Bloch-type description. A similar modification might prove effective in optical lasers as well. We have further illustrated the superiority of a periodic orbit analysis over conventional techniques with a quantitative study of a heteroclinic crisis. No applications of the symbolic dynamics to the evaluation of dimensions and entropies, via the thermodynamic formalism of nonlinear dynamics (Beck and Schlögl, 1993), have been reported, since this was beyond the scope of this review. We refer the reader to more specialistic work. Finally, a control method has been applied to the NMR laser to show how the precise location of the unstable orbits and a careful local modeling of the dynamics can be used to constrain the motion in the vicinity of a periodic orbit, in spite of its repulsivity. The method was successful for low-order orbits (up to period 4), notwithstanding the high "speed" of the system (about 100 Hz).

It appears that a careful analysis based on periodic orbits and symbolic dynamics can be helpful in understanding more general questions, such as the nature of complexity (Grassberger, 1986; Stein, 1989; Badii, 1993), at least in relatively elementary dynamical models, such as cellular automata (Wolfram, 1986), or low-dimensional maps and generalized shift transformations (Moore, 1990, 1991). These systems can be seen as surrogates of spatio-temporal chaos or even turbulence: phenomena for which, at present, no general theory exists.

Another class of systems that goes beyond that of simple low-dimensional chaos consists of delayed-feedback processes in which the future state depends on the position at the current time and at a previous one. Hence a description in terms of differential equations requires knowledge of all variables values in a whole time interval, so that the dimension of the system is infinite. This is suggestive of new phenomenology, although it can be shown that the dimension of the attractors is always bounded (Mallet-Paret, 1976). Therefore we have begun an investigation of the NMR laser with delayed feedback, as a first step toward a higher-dimensional dynamics. The dynamics exhibits quite an interesting behavior, including motion on incommensurate tori and strange attractors with dimension $D > 3$ or 4. The transition to chaos and, especially, the symbolic dynamics of such systems have not been studied yet. The experimental arrangement is obtained by rendering the quality factor Q dependent on the laser output signal, suitably delayed with an electronic device. The system is now autonomous (i.e., no external periodic forcing is needed for the onset of chaos), so that the periodic orbits do not have time lengths that are multiples of a fundamental one, and, in general, a distribution of characteristic times is expected at each given order.

ACKNOWLEDGMENTS

We gratefully acknowledge useful discussions with N. B. Abraham, D. Auerbach, P. Cvitanović, P. Grassberger, H. Haken, L. Lugiato, P. F. Meier, I. Procaccia, P. Talkner, J. Tredicce, C. Tresser, F. Waldner, and D. Walls. This work was carried out with the steady support of the Swiss National Science Foundation.

REFERENCES

Abarbanel, H. D. I., R. Brown, J. J. Sidorowich, and L. Sh. Tsimring, 1993, Rev. Mod. Phys. **65**, 1331.

Abragam, A., 1961, *The Principles of Nuclear Magnetism* (Oxford University Press, Oxford), p. 36.

Abraham, N. B., A. M. Albano, A. Passamante, and P. E. Rapp, 1989, Eds., *Measures of Complexity and Chaos* (Plenum,

New York).
Abraham, N. B., L. A. Lugiato, and L. M. Narducci, 1985, J. Opt. Soc. Am. B **2**, 7.
Adler, R. L., A. G. Konheim, and M. H. McAndrew, 1965, Trans. Am. Math. Soc. **114**, 309.
Alekseev, V. M., and M. V. Yakobson, 1981, Phys. Rep. **75**, 290.
Arecchi, F. T., R. Meucci, G. Puccioni, and J. Tredicce, 1982, Phys. Rev. Lett. **49**, 1217.
Arnold, V. I., 1964, Sov. Math. Dokl. **5**, 581.
Arnold, V. I., and A. Avez, 1968, *Ergodic Problems of Classical Mechanics* (Benjamin, New York).
Artuso, R., E. Aurell, and P. Cvitanović, 1990, Nonlinearity **3**, 325.
Auerbach, D., P. Cvitanović, J. P. Eckmann, G. Gunaratne, and I. Procaccia, 1987, Phys. Rev. Lett. **58**, 2387.
Auerbach, D., C. Grebogi, E. Ott, and J. A. Yorke, 1992, Phys. Rev. Lett. **69**, 3479.
Badii, R., 1989a, Riv. Nuovo Cimento **12**, 1.
Badii, R., 1989b, in *Measures of Complexity and Chaos,* edited by N. B. Abraham, A. M. Albano, A. Passamante, and P. E. Rapp (Plenum, New York), p. 313.
Badii, R., 1990, Europhys. Lett. **13**, 599.
Badii, R., 1993, in *Chaotic Dynamics, Theory and Practice,* edited by T. Bountis (Plenum, New York), p. 1.
Badii, R., G. Broggi, B. Derighetti, M. Ravani, S. Ciliberto, A Politi, and M. A. Rubio, 1988, Phys. Rev. Lett. **60**, 979.
Badii, R., M. Finardi, and G. Broggi, 1991, in *Chaos, Order and Patterns,* edited by P. Cvitanović, G. Casati, and R. Artuso (Plenum, New York), p. 259.
Badii, R., M. Finardi, G. Broggi, and M. A. Sepúlveda, 1992, Physica D **58**, 304.
Badii, R., and A. Politi, 1984a, Phys. Rev. Lett. **52**, 1661.
Badii, R., and A. Politi, 1984b, J. Stat. Phys. **40**, 725.
Beck, C., and F. Schlögl, 1993, *Thermodynamics of Chaotic Systems,* Cambridge Nonlinear Science Series **4** (Cambridge University, Cambridge, England).
Benedicks, M., and L. Carleson, 1991, Ann. Math. **133**, 73.
Benettin, G., L. Galgani, A. Giorgilli, and J. Strelcyn, 1980, Meccanica **15**, 9.
Bergé, P., Y. Pomeau, and C. Vidal, 1986, *Order Within Chaos* (Wiley, New York).
Billingsley, P., 1965, *Ergodic Theory and Information* (Wiley, New York).
Bösiger, P., E. Brun, and D. Meier, 1977, Phys. Rev. Lett. **38**, 602.
Bösiger, P., E. Brun, and D. Meier, 1978, Phys. Rev. A **18**, 671.
Bösiger, P., E. Brun, and D. Meier, 1979, Phys. Rev. A **20**, 1073.
Bowen, R., 1975, *Equilibrium States and the Ergodic Theory of Anosov Diffeomorphisms,* Lecture Notes in Mathematics Vol. 470 (Springer, New York).
Boyd, R. W., M. G. Raymer, and L. M. Narducci, 1986, Eds., *Optical Instabilities,* Proceedings of the International Meeting on Instabilities and Dynamics of Lasers and Nonlinear Optical Systems, Rochester, 1985 (Cambridge University, Cambridge, England).
Broggi, G., 1988, J. Opt. Soc. Am. B **5**, 1020.
Brun, E., 1991, in *Le Chaos,* 33ème cours de perfectionnement de l'Association Vaudoise des Chercheurs en Physique, edited by G. Bernasconi, A. Koch, and F. Rothen (AVCP, Lausanne), p. 147.
Brun, E., B. Derighetti, R. Holzner, and D. Meier, 1983, Helv. Phys. Acta **56**, 825.
Brun, E., B. Derighetti, R. Holzner, and D. Meier, 1984, in *Optical Bistability 2,* edited by C. M. Bowden, H. M. Gibbs, and S. L. McCall (Plenum, New York), p. 127.
Brun, E., B. Derighetti, D. Meier, R. Holzner, and M. Ravani, 1985, J. Opt. Soc. Am. B **2**, 156.
Brun, E., B. Derighetti, M. Ravani, G. Broggi, P. F. Meier, R. Stoop, and R. Badii, 1986, Phys. Scr. **T13**, 119.
Chaos, 1992, "Focus" edition on periodic orbit theory, Chaos **2**, No. 1.
Chirikov, B. V., 1979, Phys. Rep. **52**, 263.
Collet, P., and J.-P. Eckmann, 1980, *Iterated Maps on the Interval as Dynamical Systems* (Birkhäuser, Cambridge, MA).
Cornfeld, I. P., S. V. Fomin, and Ya. G. Sinai, 1982, *Ergodic Theory* (Springer, New York).
Crutchfield, J. P., and K. Young, 1989, Phys. Rev. Lett. **63**, 105.
Cvitanović, P., 1984, Ed., *Universality in Chaos* (Hilger, Bristol).
Cvitanović, P., 1988, Phys. Rev. Lett. **61**, 2729.
D'Alessandro, G., and A. Politi, 1989, Phys. Rev. Lett. **64**, 1609.
Derighetti, B., M. Ravani, R. Stoop, P. F. Meier, E. Brun, and R. Badii, 1985, Phys. Rev. Lett. **55**, 17.
Ditto, W. L., S. N. Rauseo, R. Cawley, C. Grebogi, G.-H. Hsu, E. Kostelich, E. Ott, H. T. Savage, R. Segnan, M. L. Spano, and J. A. Yorke, 1989, Phys. Rev. Lett. **63**, 923.
Ditto, W. L., S. N. Rauseo, and M. L. Spano, 1990, Phys. Rev. Lett. **65**, 3211.
Drazin, P. G., and G. P. King, 1992, Eds., *Interpretation of Time Series from Nonlinear Dynamics* (Elsevier, Amsterdam).
Eckmann, J.-P., S. O. Kamphorst, D. Ruelle, and S. Ciliberto, 1986, Phys. Rev. A **34**, 4971.
Eckmann, J.-P., and I. Procaccia, 1986, Phys. Rev. A **34**, 659.
Eckmann, J.-P., and D. Ruelle, 1985, Rev. Mod. Phys. **57**, 617.
Farmer, J. D., and J. J. Sidorowich, 1987, Phys. Rev. Lett. **59**, 845.
Feigenbaum, M. J., 1978, J. Stat. Phys. **19**, 25.
Feigenbaum, M. J., 1979, J. Stat. Phys. **21**, 669.
Feigenbaum, M. J., 1980, Los Alamos Sci. **1**, 4.
Feigenbaum, M. J., 1988, J. Stat. Phys. **52**, 527.
Feigenbaum, M. J., M. H. Jensen, and I. Procaccia, 1986, Phys. Rev. Lett. **57**, 1503.
Feigenbaum, M. J., I. Procaccia, and T. Tél, 1989, Phys. Rev. A **39**, 5359.
Finardi, M., 1993, Ph.D. thesis (Zürich University).
Finardi, M., L. Flepp, J. Parisi, R. Holzner, R. Badii, and E. Brun, 1992, Phys. Rev. Lett. **68**, 2989.
Flepp, L., 1991, Ph.D. thesis (Zürich University).
Flepp, L., R. Holzner, E. Brun, and C. Broens, 1990, in *Proceedings of the 25th Congress Ampère on Magnetic Resonance and Related Phenomena, Stuttgart,* edited by M. Mehring, J. U. Schütz, and H. C. Wolf (Springer-Verlag, Berlin), p. 391.
Flepp, L., R. Holzner, E. Brun, M. Finardi, and R. Badii, 1991, Phys. Rev. Lett. **67**, 2244.
Giovannini, F., and A. Politi, 1991, J. Phys. A **24**, 1837.
Giovannini, F., and A. Politi, 1992, Phys. Lett. A **161**, 332.
Grasiuk, A. Z., and A. N. Oraevskij, 1964, in *Quantum Electronics and Coherent Light,* Proceedings of the International Fermi School, Course XXXI (1963), edited by P. A. Miles (Academic, New York), p. 203.
Grassberger, P., 1986, Int. J. Theor. Phys. **25**, 907.
Grassberger, P., R. Badii, and A. Politi, 1988, J. Stat. Phys. **51**, 135.
Grassberger, P., R. Hegger, H. Kantz, C. Schaffrath, and T. Schreiber, 1993, Chaos **3**,127.
Grassberger, P., and H. Kantz, 1985, Phys. Rev. A **113**, 235.

Grassberger, P., H. Kantz, and U. Moenig, 1990, J. Phys. A **22**, 5217.
Grassberger, P., and I. Procaccia, 1983, Phys. Rev. Lett. **50**, 346.
Grassberger, P., and I. Procaccia, 1984, Physica D **13**, 34.
Grassberger, P., T. Schreiber, and C. Schaffrath, 1991, Int. J. Bifurc. Chaos **1**, 521.
Grebogi, C., E. Ott, F. Romeiras, and J. A. Yorke, 1987, Phys. Rev. A **36**, 5365.
Grebogi, C., E. Ott, and J. A. Yorke, 1987, Phys. Rev. A **36**, 3522.
Grebogi, C., E. Ott, and J. A. Yorke, 1988, Phys. Rev. A **37**, 1711.
Guckenheimer, J., and P. Holmes, 1986, *Nonlinear Oscillations, Dynamical Systems, and Bifurcations of Vector Fields,* Applied Mathematical Sciences Vol. 42, 2nd ed. (Springer, New York).
Gunaratne, G. H., M. H. Jensen, and I. Procaccia, 1988, Nonlinearity **1**, 157.
Haken, H., 1975, Phys. Lett. A **53**, 77.
Haken, H., 1981, Ed., *Chaos and Order in Nature,* Springer Series in Synergetics Vol. 11 (Springer, Berlin).
Halsey, T. C., M. H. Jensen, L. P. Kadanoff, I. Procaccia, and B. Shraiman, 1986, Phys. Rev. A **33**, 1141.
Hénon, M., 1976, Commun. Math. Phys. **50**, 69.
Holzner, R., B. Derighetti, M. Ravani, and E. Brun, 1987, Phys. Rev. A **36**, 3.
Kantz, H., T. Schreiber, I. Hoffmann, T. Buzug, G. Pfister, L. Flepp, J. Simonet, R. Badii, and E. Brun, 1993, Phys. Rev. E **48**, 1529.
Kolmogorov, A. N., 1954, Dokl. Akad. Nauk SSSR **98**, 527.
Kostelich, E. J., and H. L. Swinney, 1987, in *Chaos and Related Nonlinear Phenomena,* edited by I. Procaccia and M. Shapiro (Plenum, New York), p. 118.
Kostelich, E. J., and J. A. Yorke, 1988, Phys. Rev. A **38**, 1649.
Lathrop, D. P., and E. J. Kostelich, 1989, Phys. Rev. A **40**, 4028.
Lewin, B., 1990, *Genes IV* (Oxford University Press, New York).
Libchaber, A., and J. Maurer, 1979, J. Phys. (Paris) Colloq. **41**, C3-51.
Lichtenberg, A. J., and M. A. Lieberman, 1992, *Regular and Chaotic Dynamics,* Applied Mathematical Sciences Vol. 38, 2nd ed. (Springer, New York).
Lorenz, E. N., 1963, J. Atmos. Sci. **20**, 130.
MacKay, R. S., and J. D. Meiss, 1987, Eds., *Hamiltonian Dynamical Systems: A Reprint Selection* (Hilger, Bristol).
Mallet-Paret, J., 1975, J. Differ. Eq. **22**, 331.
Mandelbrot, B. B., 1982, *The Fractal Geometry of Nature* (Freeman, San Francisco).
Mayer, D. H., 1991, in *Ergodic Theory, Symbolic Dynamics and Hyperbolic Spaces,* edited by T. Bedford, M. Keane, and C. Series (Oxford University Press, New York), p. 175.
Mayer-Kress, G., 1986, Ed., *Dimensions and Entropies in Chaotic Systems* (Springer, Berlin); 2nd printing, 1989.
McCauley, J. L., 1993, *Chaos, Dynamics and Fractals,* Cambridge Nonlinear Science Series Vol. 2 (Cambridge University, Cambridge, England).
Metropolis, M., M. L. Stein, and P. R. Stein, 1973, J. Combin. Theory **15**, 25.
Mézard, M., G. Parisi, and M. A. Virasoro, 1987, *Spin Glass Theory and Beyond* (World Scientific, Singapore).
Mindlin, G. B., and R. Gilmore, 1992, in *Interpretation of Time Series from Nonlinear Dynamics,* edited by P. G. Drazin and G. P. King (Elsevier, Amsterdam), p. 229.
Mindlin, G. B., X. J. Hou, H. G. Solari, R. Gilmore, and N. B. Tufillaro, 1990, Phys. Rev. Lett. **64**, 2350.
Moore, C., 1990, Phys. Rev. Lett. **64**, 2354.
Moore, C., 1991, Nonlinearity **4**, 199.
Moser, J., 1973, *Stable and Random Motions in Dynamical Systems* (Princeton University, Princeton, NJ).
Nakamura, K., 1993, *Quantum Chaos, A New Paradigm of Nonlinear Dynamics,* Cambridge Nonlinear Science Series Vol. 3 (Cambridge University, Cambridge, England).
Newhouse, S. E., 1974, Topology **13**, 9.
Oseledec, V. I., 1968, Trans. Moscow Math. Soc. **19**, 197.
Ott, E., C. Grebogi, and J. A. Yorke, 1990a, Phys. Rev. Lett. **64**, 1196.
Ott, E., C. Grebogi, and J. A. Yorke, 1990b, in *Chaos: Soviet-American Perspectives on Nonlinear Science,* edited by D. K. Campbell (American Institute of Physics, New York), p. 153.
Packard, N. H., J. P. Crutchfield, J. D. Farmer, and R. S. Shaw, 1980, Phys. Rev. Lett. **45**, 712.
Pawelzik, K., and H. G. Schuster, 1991, Phys. Rev. A **43**, 1808.
Pesin, Ya. B., 1976, Sov. Math. Dokl. **17**, 196.
Poincaré, H., 1892, *Les Méthodes, Nouvelles de la Mécanique Céleste* (Gauthier-Villars, Paris).
Pollicott, M., 1991, in *Ergodic Theory, Symbolic Dynamics and Hyperbolic Spaces,* edited by T. Bedford, M. Keane, and C. Series (Oxford University Press, New York), p. 153.
Ravani, M., B. Derighetti, G. Broggi, E. Brun, and R. Badii, 1988, J. Opt. Soc. Am. B **5**, 1029.
Renyi, A., 1970, *Probability Theory* (North-Holland, Amsterdam).
Reyl, C., L. Flepp, R. Badii, and E. Brun, 1993, Phys. Rev. E **47**, 267.
Ruelle, D., 1978, *Thermodynamic Formalism,* Vol. 5 of Encyclopedia of Mathematics and Its Applications (Addison-Wesley, Reading, MA).
Ruelle, D., and F. Takens, 1971, Commun. Math. Phys. **20**, 167.
Sargent, M., III, M. O. Scully, and W. E. Lamb, Jr., 1974, *Laser Physics* (Addison-Wesley, Reading, MA).
Šarkovskii, A. N., 1964, Ukr. Mat. Zh. **16**, 61.
Sauer, T., J. A. Yorke, and M. Casdagli, 1991, J. Stat. Phys. **65**, 579.
Schuster, H. G., 1988, *Deterministic Chaos* (VCH, Weinheim, Germany).
Shilnikov, L. P., 1970, Mat. Sb. **81**, 92 and 123.
Sinai, Ya. G., 1972, Russ. Math. Surv. **27**, 21.
Smale, S., 1967, Bull. Am. Math. Soc. **73**, 747.
Sommerer, J. C., W. L. Ditto, C. Grebogi, E. Ott, and M. L. Spano, 1991a, Phys. Lett. A **153**, 105.
Sommerer, J. C., W. L. Ditto, C. Grebogi, E. Ott, and M. L. Spano, 1991b, Phys. Rev. Lett. **66**, 1947.
Stein, D. L., 1989, Ed., *Lectures in the Sciences of Complexity,* Santa Fe Institute (Addison-Wesley, Reading, MA).
Swinney, H. L., and J. P. Gollub, 1981, Eds., *Hydrodynamic Instabilities and the Transitions to Turbulence* (Springer, New York).
Takens, F., 1980, in *Dynamical Systems and Turbulence,* edited by D. A. Rand and L.-S. Young, Lecture Notes in Mathematics 898 (Springer-Verlag, Berlin), p. 366.
Tél, T., 1988, in *Directions in Chaos,* edited by B. L. Hao (World Scientific, Singapore), Vol. 3, p. 149.
Tufillaro, N. B., R. Holzner, L. Flepp, M. Finardi, and R. Badii, 1991, Phys. Rev. A **44**, R4786.
Tufillaro, N. B., J. P. Reilly, and T. A. Abbot, 1991, *An Experimental Approach to Nonlinear Dynamics and Chaos* (Addison-Wesley, New York).

Walters, P., 1985, *An Introduction to Ergodic Theory,* 2nd. ed. (Springer, New York).
Wolfram, S., 1986, *Theory and Applications of Cellular Automata* (World Scientific, Singapore).
Young, L.-S., 1982, Ergodic Theory Dyn. Syst. **2**, 109.
Zaslavsky, G. M., R. Z. Sagdeev, D. A. Usikov, and A. A. Chernikov, 1991, *Weak Chaos and Quasi-Regular Patterns,* Cambridge Nonlinear Science Series Vol. 1 (Cambridge University, Cambridge, England).